Biochimica et Biophysica Acta 1817 (2012) 1164–1176

Contents lists available at SciVerse ScienceDirect

Biochimica et Biophysica Acta

journal homepage: www.elsevier.com/locate/bbabio

Mechanism of light induced water splitting in Photosystem II of oxygen evolving photosynthetic organisms ☆

Gernot Renger *

Technical University Berlin, Institute Chemistry, Max-Volmer-Laboratory of Biophysical Chemistry, Straße des 17. Juni 135, D-10623 Berlin, Germany

ARTICLE INFO

Article history:
Received 16 December 2011
Received in revised form 27 January 2012
Accepted 5 February 2012
Available online 12 February 2012

Keywords:
Photosystem II watersplitting
Hydrogen bond network
Redox isomerism
Proton tautomerism
Non-adiabatic electron transfer
O – O bond formation

ABSTRACT

The reactions of light induced oxidative water splitting were analyzed within the framework of the empirical rate constant–distance relationship of non-adiabatic electron transfer in biological systems (C. C. Page, C. C. Moser, X. Chen , P. L. Dutton, Nature 402 (1999) 47–52) on the basis of structure information on Photosystem II (PS II) (A. Guskov, A. Gabdulkhakov, M. Broser, C. Glöckner, J. Hellmich, J. Kern, J. Frank, W. Saenger, A. Zouni, Chem. Phys. Chem. 11 (2010) 1160–1171, Y. Umena, K. Kawakami, J-R Shen, N. Kamiya, Crystal structure of oxygen-evolving photosystem II at a resolution of 1.9 Å. Nature 47 (2011) 55–60). Comparison of these results with experimental data leads to the following conclusions: 1) The oxidation of tyrosine Y_z by the cation radical $P680^{+\cdot}$ in systems with an intact water oxidizing complex (WOC) is kinetically limited by the non-adiabatic electron transfer step and the extent of this reaction is thermodynamically determined by relaxation processes in the environment including rearrangements of hydrogen bond network(s). In marked contrast, all Y_z^{ox} induced oxidation steps in the WOC up to redox state S_3 are kinetically limited by trigger reactions which are slower by orders of magnitude than the rates calculated for non-adiabatic electron transfer. 3) The overall rate of the triggered reaction sequence of Y_z^{ox} reduction by the WOC in redox state S_3 eventually leading to formation and release of O_2 is kinetically limited by an uphill electron transfer step. Alternative models are discussed for this reaction. The protein matrix of the WOC and bound water molecules provide an optimized dynamic landscape of hydrogen bonded protons for catalyzing oxidative water splitting energetically driven by light induced formation of the cation radical $P680^{+\cdot}$. In this way the PS II core acts as a molecular machine formed during a long evolutionary process. This article is part of a Special Issue entitled: Photosynthesis Research for Sustainability: from Natural to Artificial.

1. Introduction

Photosynthetic water splitting into molecular dioxygen and hydrogen bound to suitable acceptor molecules is the key process of solar energy exploitation by the biosphere. The molecular machinery that enables the efficient performance of this reaction was “invented” 2–3 billion years ago at the level of ancient cyanobacteria thus opening the way for the development of all higher forms of life on our planet (for a recent review, see Ref. [1]). The essential steps of light induced water splitting in photosynthetic organisms take place in a special system: the multimeric complex of Photosystem II (PS II) which is anisotropically incorporated into the thylakoid membrane and acting as water-plastoquinone:oxido-reductase [2]. PS II consists of a comparatively large number of more than 20 subunits [3,4]. From an evolutionary point of view, it is intriguing that the PS II complex evolved in a strikingly narrow window of geological time and that the composition of cofactors as well as of polypeptides is surprisingly invariant to evolutionary development [5]. The PS II complex is nature's unique masterpiece for biological solar energy exploitation by photosynthetic water splitting and therefore also of great interest for all considerations on the construction of technical devices for the use of solar radiation as Gibbs free energy source [6,7].

The overall reaction pattern of PS II comprises three different types of processes: (i) light induced charge separation into an ion radical pair $P680^{+\cdot}Q_A^{-\cdot}$ [2], (ii) oxidative water splitting into molecular dioxygen and four protons via a sequence of four redox steps, and (iii) two step reduction of plastoquinone to plastoquinol under proton uptake [8].

Fig. 1 shows the structural arrangement of the cofactors that are involved in these reactions (for further details, see [9]).

The general scheme of reaction sequences (i) and (iii) leading to formation of $P680^{+\cdot}Q_A^{-\cdot}$ and plastoquinol, respectively, and the structural array of the cofactors involved are not special characteristics of PS II but resemble those of the corresponding reactions taking place in type II reaction centers of anoxygenic photosynthetic bacteria [10,11]. On the other hand, the reaction sequence (ii) of $P680^{+\cdot}$ driven oxidative water splitting is the unique process of all oxygen evolving

☆ This article is part of a Special Issue entitled: Photosynthesis Research for Sustainability: from Natural to Artificial.

* Tel.: +49 30 314 22794; fax: +49 30 314 211 22.
E-mail address: gernot.renger@mailbox.tu-berlin.de.

0005-2728/$ – see front matter © 2012 Elsevier B.V. All rights reserved.
doi:10.1016/j.bbabio.2012.02.005

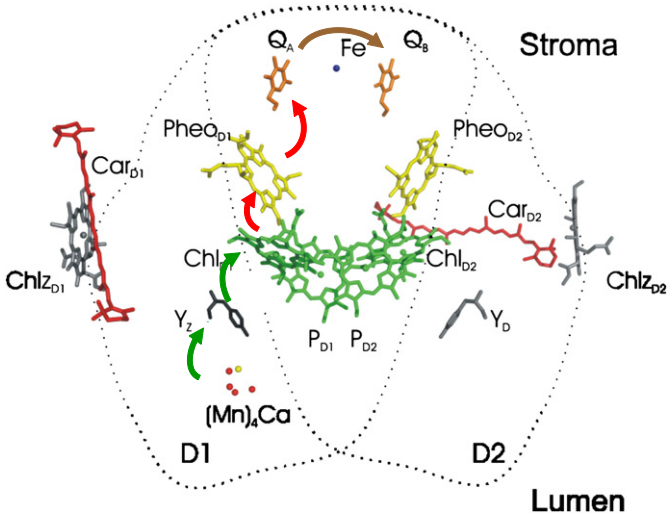

Fig. 1. Side view of the structural array of the cofactors within the heterodimer of polypeptides D1 and D2. Chl_{D1}, Chl_{D2}, P_{D1} and P_{D2} (marked in green) are the four chlorophyll *a* (Chl *a*) and $Pheo_{D1}$ and $Pheo_{D2}$ (marked in yellow) the two pheophytin *a* (Pheo *a*) molecules of the reaction center pigments core. Chl z_{D1} and Chl z_{D2}, the distal Chl *a* molecules and two carotenoids Car_{D1} and Car_{D2} (marked in red) ; Q_A, plastoquinone acceptor; the $Mn)_4O_xCa$ cluster of the water oxidizing complex is symbolized by a green circle area (the four manganese are marked in red, the single Ca in yellow); and Fe is the non heme iron center. The dimensions of D1 and D2 are symbolized by dotted contour lines. The reaction sequences i, ii and iii are symbolized by arrows in red, green and brown, respectively. The data was kindly provided by Jan Kern. For details see text.

photosynthetic organisms. The present study is exclusively dealing with this process.

Before analyzing the mechanism of light induced oxidative water splitting a few basic properties of the redox system $H_2O/O_2 + 4H^+$ in aqueous solution and in PS II will be briefly summarized. The upper panels of Fig. 2 present schemes of the sequence of 1-electron/1-proton redox steps leading from water to O_2 and vice versa (left side) and of the energetics of these reactions in aqueous solution (right side). Inspection of these schemes readily reveals two important features: a) the four step sequence comprises the reactive oxygen species (ROS) $HO^{\cdot}$, H_2O_2 and $HO_2/O_2^{-\cdot}$ which are harmful to biological systems and therefore populations of these intermediates have to be suppressed when performing this process in sensitive biological systems, and b) the standard Gibbs free energy gap ΔG^0 is quite different for the individual reactions [12], in particular the first 1-electron redox step of oxidative water splitting is highly endergonic and cannot be driven by the energy of a photon in the red wavelength region.

Both problems, i.e. "taming" of the reaction sequence and a proper tuning of its energetics have been solved by "nano-scale encapsulation" of the process into a protein bound transition metal cluster. It is most important to note that nature has not only evolved two entirely different devices to catalyze the reaction in the forward (water oxidizing complex (WOC) of PS II) and backward (cytochrome *c* oxidase of the respiratory chain) direction but also that these enzymes function in a unidirectional manner. Another striking feature is the invariance of the catalytic centers to evolutionary development from ancient primitive prokaryotic organisms to higher plants and animals [1].

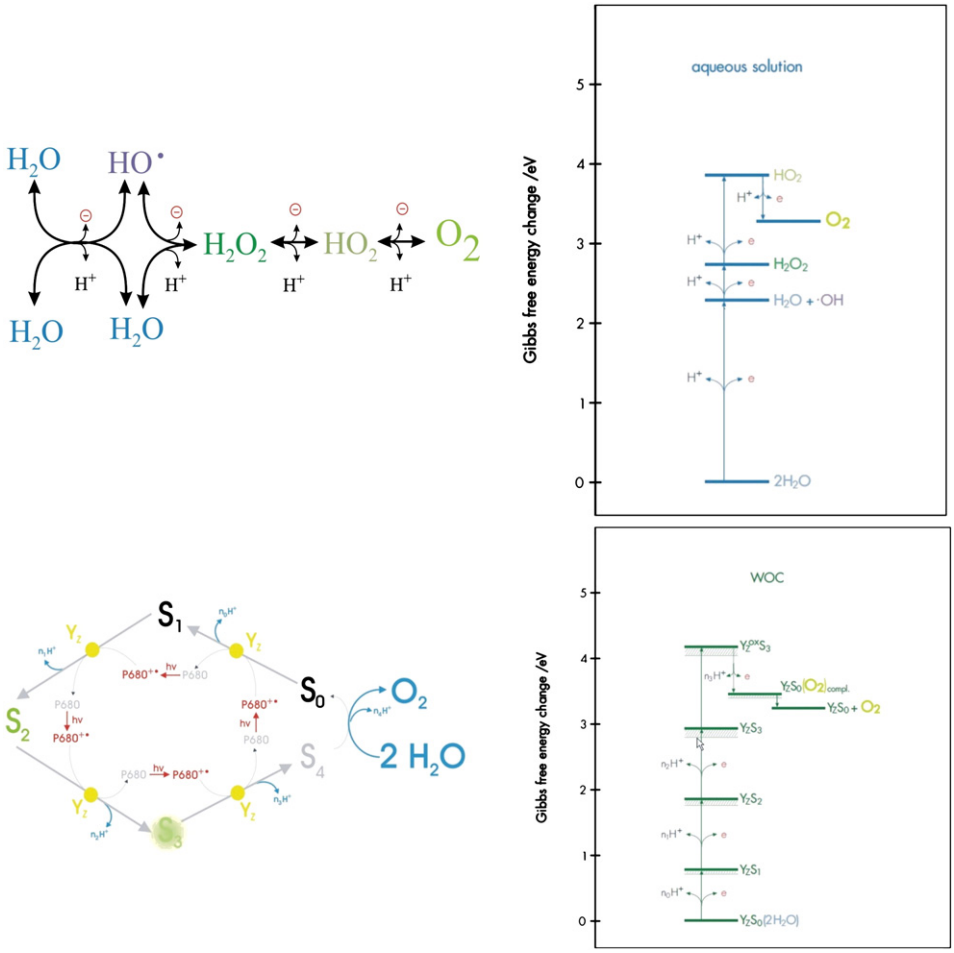

Fig. 2. Reaction scheme (left side) and energetics (right side) of stepwise oxidative water splitting in aqueous solution (top panels) and in Photosystem II (bottom panels. For details see text.

The bottom panel of Fig. 2 shows the general pattern of the reaction sequence of oxidative water spitting in PS II (left side) and its energetics (right side). Inspection of the two reaction schemes on the left side reveals that oxidative water splitting in both, aqueous solution (upper panel) and the WOC of PS II (lower panel) comprises five states where S_0 and S_4 of the WOC reflect the redox levels of H_2O and O_2, respectively, and the three intermediary states S_1, S_2 and S_3 only formally correspond with the redox levels of hydroxyl radical, peroxide and superoxide, respectively. A comparison of the energetics reveals that S_1, S_2 and S_3 are intermediates which significantly differ from those species that are transiently populated in aqueous solution due to the "taming" of the process by linking the reactions to redox active manganese at the catalytic site of the WOC (for an earlier discussion of this most important point, see [13]). A striking feature of the reactions taking place in the WOC of PS II is the remarkable tuning of the energetics of the individual redox steps which are characterized by a very similar Gibbs free energy gap of about 1 eV, except of the transition $S_0 \rightarrow S_1$ with a markedly lower value (for a discussion of the energetics of this particular redox step and their possible physiological implications, see [14]).

The reaction sequence of the WOC is driven by the strongly oxidizing cation radical $P680^{+\cdot}$, formed as a result of the light induced charge separation via reaction sequence (i), and mediated by component Y_z[2] which was identified as the tyrosine residue Y161 of polypeptide D1 [15,16]. The structural array of the cofactors involved in oxidative water splitting reveals that Y_z is not a constituent of the catalytic site itself because its distance to the redox active metal centers of the WOC is about 7 Å [17,18]. Accordingly, two types of reactions have to be analyzed in order to unravel the mechanism of oxidative water splitting in PS II: (A) oxidation of Y_z by $P680^{+\cdot}$ which also takes place – but with altered kinetics – when the WOC is lacking (see section *Oxidation of Y_z by $P680^{+\cdot}$*) and (B) sequence of oxidation steps at the catalytic site of the WOC with Y_z^{ox} acting as the oxidant. Both types of reactions comprise the participation of protonatable redox groups and therefore the mode of coupling between proton transfer (PT) and electron transfer (ET) is of high mechanistic relevance (for reviews on the fundamental role of this mode of coupling in biological redox reactions and theoretical considerations on the mechanism, see [19–22]). The cofactors of the WOC and Y_z are functionally and structurally linked together via hydrogen bond networks [18].

The present investigations are focused on reactions (A) and (B) by analyzing on the basis of structure information the available kinetic data within the framework of the Marcus theory of nonadiabatic electron transfer thus leading to important conclusions on the mechanism.

2. Data analyses

The rate constants $k_{f,i}^{NET}$ of nonadiabatic electron transfer (NET) reactions between the initial (i) and the final (f) state are obtained by using the "classical" Marcus–Levich–Hush relation (for a review, see [23])

$$k_{f,i}^{NET} = \frac{2\pi}{\hbar}\left|V_{f,i}(R_{DA})\right|^2\left(4\pi\lambda_{f,i}k_BT\right)^{-1/2}\exp\left\{-\left(\Delta G_{f,i}^0+\lambda_{f,i}\right)^2/4\lambda_{f,i}k_BT\right\} \quad (1)$$

where $V_{f,i}(R_{DA})$ and R_{DA} are the matrix element of electronic coupling and the edge to edge distance, respectively, between electron donor and acceptor group, $\Delta G_{f,i}^0$ the Gibbs free energy gap between $D^{red}A^{ox}$ (state i) and $D^{ox}A^{red}$ (state f) $\lambda_{f,i}$ the reorganization energy, $h = 2\pi\hbar$ the Planck constant and k_B the Boltzmann constant.

An empirical rate constant–distance relationship of the type

$$\log k_{f,i}^{NET} = 13-(1.2-0.8\rho)(R_{DA}-3.6)-3.1\left(\Delta G_{f,i}^0+\lambda_{f,i}\right)^2/\lambda_{f,i} \quad (2)$$

has been derived for $k_{f,i}^{NET}$ on the basis of the relation $|V_{f,i}(R_{DA})|^2 = |V_{f,i}(R_{DA}=0)|^2\exp(-\beta\cdot R_{DA})$ with $\beta = \rho\,0.9\,Å^{-1}+(1-\rho)\,2.8\,Å^{-1}$ (for details, see [24]) where ρ is the packing density of protein atoms between the redox centers (ρ varies between 0 for vacuum and 1 for full package).

The values of $(\Delta G_{f,i}^0+\lambda_{f,i})^2/\lambda_{f,i}$ in Eq. (2) are gathered from the experimental activation energies $E_{A,f/i}$ (see [25]):

$$\left(\Delta G_{f,i}^0+\lambda_{f,i}\right)^2/\lambda_{f,i} = 4\left(E_{A,f,i}+0.5\ RT\right). \quad (3)$$

The evaluation of kinetic schemes for the reduction of Y_z^{ox} by the WOC in redox state S_3 was performed by numerical integration of the system of linear differential equations using self written algorithms in C#. This algorithm was provided by Dr. M. Vitali.

3. Results and discussion

3.1. Oxidation of Y_z by $P680^{+\cdot}$

Based on the binding of the cofactors in a well defined geometry (distance, mutual orientation) within the heterodimeric D1/D2 protein matrix [17,18,26] $P680^{+\cdot}$ reduction by Y_z could be expected to exhibit a mono-exponential kinetics. However, this was found not to be the case because all types of samples with a functionally competent WOC analyzed so far (PS II core complexes from cyanobacteria and spinach, PS II membrane fragments, thylakoids and whole leaves) exhibit characteristic multi-phasic kinetics which depend on the redox state of the WOC [27–33]. These kinetics can be approximately described by the sum of three mono-exponential components with half life times of 20–50 ns, 300–600 ns and 30–40 μs, referred to as "fast ns", "slow ns" and "35 μs" kinetics, respectively, (for details, see [32]) and explained by two alternative models: a) "static" sample heterogeneity (an ensemble of PS II complexes with different structural features and/or energetic parameters, e.g. distribution of distances between Y_Z and P680 and/or Gibbs free energy gap/reorganizatio energy, respectively) or b) "dynamic" transitions through a sequence of redox equilibria of the type $[P680^{+\cdot}Y_z \Leftrightarrow P680Y_Z^{OX}]_j$ due to relaxation processes (index j symbolizes a particular stage of the sequence) analogous to those discussed for the radical pairs of light induced charge separation leading to $P680^{+\cdot}Pheo^{-\cdot}$ and subsequent formation of $P680^{+\cdot}Q_A^{-\cdot}$ (for details see [34]).

In the case of "static" heterogeneity at energetic homogeneity, a distance enlargement by about 1.7 Å and 4.8 Å relative to that of the state with a "fast ns" kinetics would be required to cope with the "slow ns" and "35 μs" kinetics, respectively (see Eq. (2)). This idea can be readily excluded on the basis of available structure information [17,18,26]. Alternatively, an increase of the activation energy by about 6 kJ/mol and 18 kJ/mol in complexes with "slow ns" and "35 μs" kinetics, respectively, compared to complexes with "fast ns" kinetics could explain the experimental data in case of homogeneity of the mutual geometry of $P680^{+\cdot}$ and Y_z (see Eqs. (2) and (3)). Furthermore, a combination of both structural and energetic effects has to be taken into account. However, regardless of the details of the mode of a "static" heterogeneity, the population probability of PS II complexes with definitely different activation energies/structural parameters must be dependent on the redox state of the WOC. A phenomenon of this type, however, is difficult to rationalize and therefore this model is inferred to be highly unlikely.

Based on these brief considerations a sequence of relaxation processes is assumed to be responsible for the multi-phasic kinetics of $P680^{+\cdot}$ reduction by Y_z, in line with our former proposal [32]. The top panel of Fig. 3 shows that the redox reaction which involves PT and ET is a multistate proton and electron transfer (MS-PET) process where the involved PT and ET step each comprises different atoms (for a general discussion, see [21]). Subsequent relaxation processes

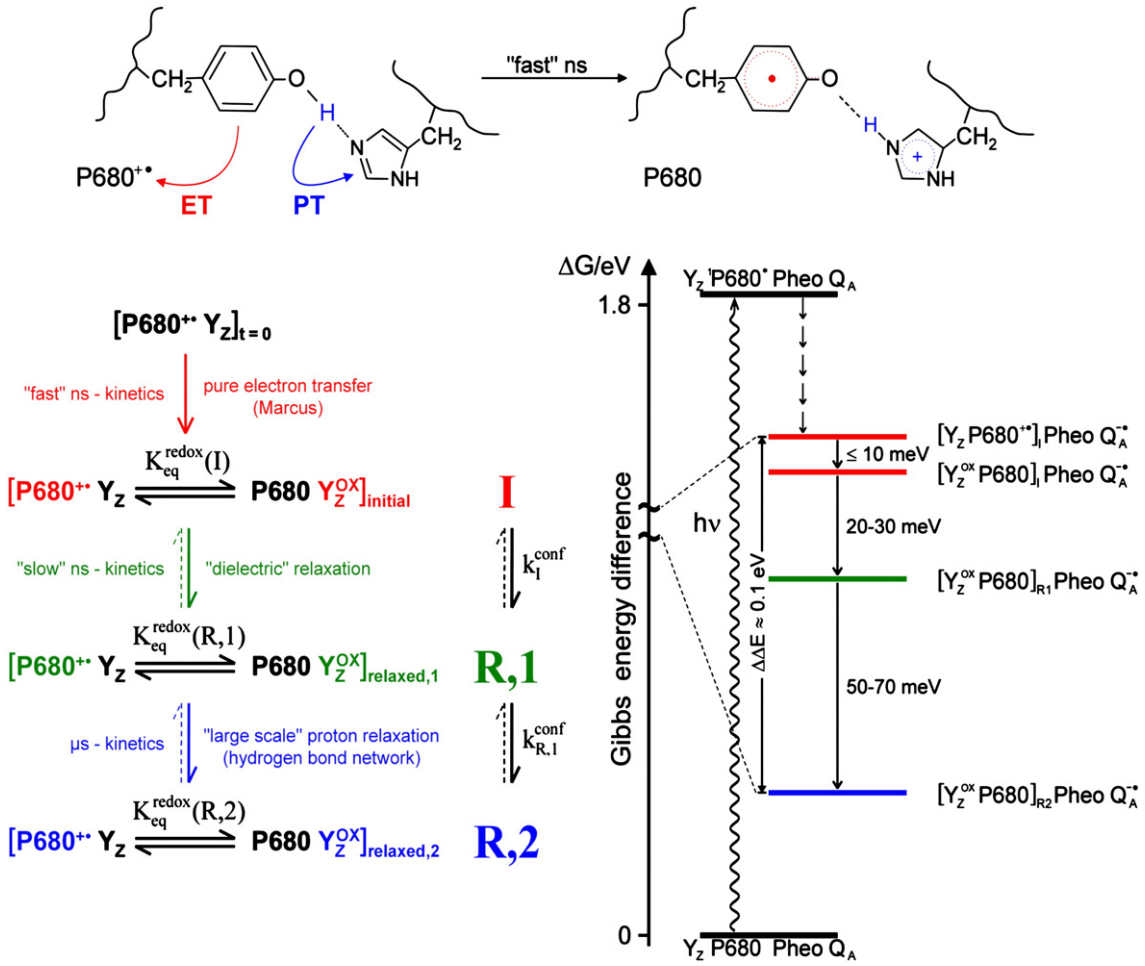

Fig. 3. Top panel: scheme of proton coupled electron transfer (top panel)Bottom panel: simplified reaction sequence (left side) and corresponding energetics (right side) of $P680^{+\bullet}$ reduction by Y_Z in PS II complexes with intact water-oxidizing complex (WOC) in redox state S_1. The initial state I and the two relaxed states R,1 and R,2 are marked in red (I), green (R,1) and blue (R, 2). For details, see text.

in the environment are assumed to cause a shift of the equilibrium constant K_j towards larger values thus giving rise to the "slow ns" and "35 µs" kinetics. The left panel of the bottom part presents a scheme of the reaction pattern and the right panel describes the corresponding energetics of the ladder of states (for further details see [32]). This scheme relates to the "3-phase approximation" of the $P680^{+\cdot}$ reduction kinetics (vide supra) but it can be easily extended to cover more complex multi-phasic kinetics.

As a consequence of the model of "dynamic" transitions (see Fig. 3), only the "fast ns" kinetics reflect the properties of the redox step leading to $P680^{+\cdot}$ reduction by Y_Z. Therefore this reaction will be analyzed in more detail. The activation energy was found to be about 10 kJ/mol on PS II membrane fragments from spinach with the WOC attaining the redox state S_1[29]. Slightly higher values were obtained for PS II core complexes from both cyanobacteria and higher plants [32,35] Evaluation of the experimental rate constant and activation energy within the framework of Eqs. (1)–(3) leads to a reorganization energy of 0.6 ± 0.1 eV thus confirming former calculations (0.5 eV) [36]. An edge to edge distance of 10 ± 1 Å is obtained by using Eqs. (2) and (3) with a value of $\rho = 0.76$ (see [24]). This "calculated" distance is in perfect agreement with 9.6 Å gathered from X ray diffraction crystallographic (XRDC) data [17,18] and is also in line with our previously reported value of 9 ± 2 Å [37].

The striking correspondence of the "calculated" and experimental distance values is a mechanistically important result because it implies that the "fast ns" kinetics of $P680^{+\cdot}$ reduction by Y_Z can be perfectly described by the "theoretical" rate constant of a nonadiabatic electron transfer step. As a consequence, the rate of this reaction step is neither limited by any trigger reaction nor by the coupled proton transfer which was proposed to comprise a shift within the hydrogen bond between the phenolic OH group of Y_z and an acceptor base B [29]. This idea is in line with the finding that the isotope effect (KIE) of the "fast ns" kinetics due to replacement of exchangeable protons by deuterons is negligibly small ($k_H/k_D < 1.05$) [38]. The base B was identified as His 190 by both mutagenesis studies (see [39] and references therein) and XRDC structure analyses [17,18,26].

New information on the mode of hydrogen bonding of Y_z were gathered from the 1.9 Å XRDC structure [26] revealing that the phenolic OH group of Y_z not only interacts with His 190 but in addition with two water molecules that are part of a hydrogen bond network which also comprises the contact with metal centers of the catalytic site of the WOC [18,26]. Quantum mechanical/molecular mechanical (QM/MM) calculations show that the water molecules form a cluster near Y_z and play a key role in determining the short distance between the phenolic oxygen atom of reduced Y_z and the N_ε atom of His 190 [40]. The electron abstraction from Y_z by $P680^{+\cdot}$ has been assumed to give rise to a rearrangement of the hydrogen bond network (see [32] and references therein). This conclusion is supported by the new QM/MM calculations revealing a lengthening of the distance between the O-atom of oxidized Y_z and the His 190 N_ε atom ([40]).

The mode of hydrogen bonding is expected to be different in redox states S_0 and S_1 versus S_2 and S_3 because the latter two redox states are characterized by the surplus of a positive charge [41]. The altered hydrogen bond network and the localization of the surplus

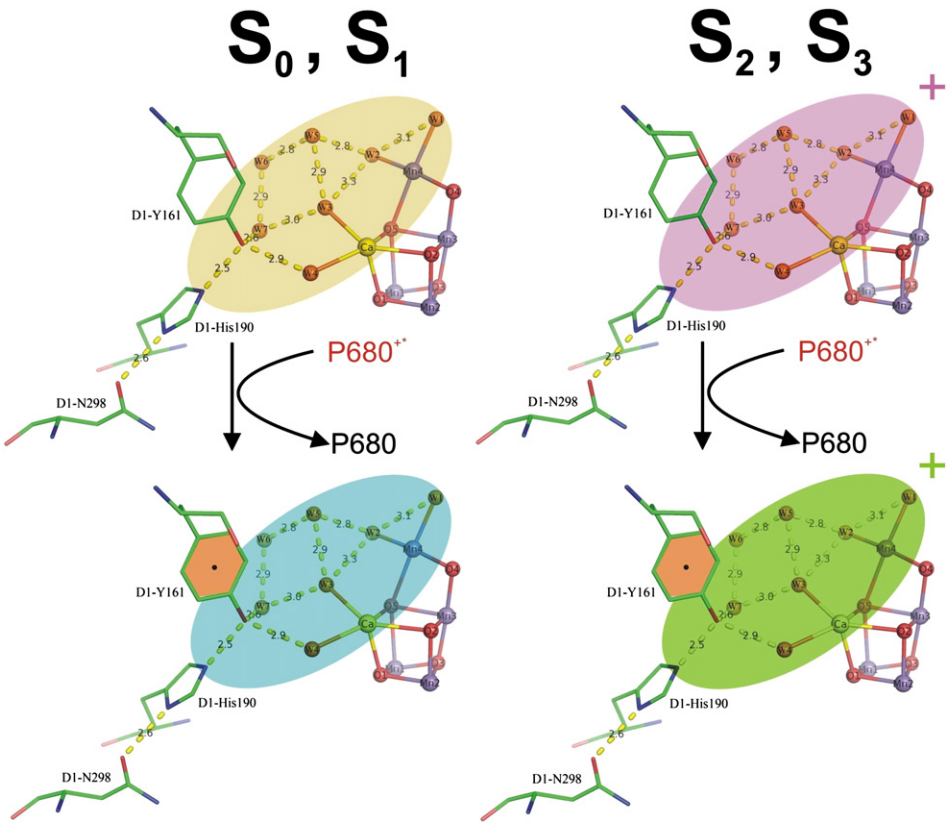

Fig. 4. Schematic representation of the hydrogen bond network in the environment of Y_z (D1-Y161). The differently colored ellipses symbolize different arrangements of individual hydrogen bonds within the network due to oxidation of Y_z (marked in orange, see bottom panels) and the surplus of a positive charge in S_2 and S_3 (right panels). For further details, see text.

charge are inferred to be responsible for the different equilibrium constants K_j which determines the normalized amplitudes of the "fast ns", "slow ns" and "35 μs" kinetics (see Fig. 3, bottom part).

Fig. 4 schematically illustrates the changes of the hydrogen bond network coupled with Y_z oxidation and the differences due to the redox state of the WOC. It must be emphasized that no structure information is available on the details of hydrogen bonding in the individual redox states S_i. Therefore the 1.9 Å structure was used only as a frame and the presumed changes due to the Y_z turnover during the S_i state transitions are symbolized by differently colored ovals.

The crucial role of hydrogen bonding is reflected by the finding that Y_z can be oxidized by $P680^{+\cdot}$ at 5 K in samples with an intact WOC in redox states S_0 and S_1 while significantly higher temperatures are required for the WOC in S_2[42,43].

The close interaction with the catalytic Mn_4O_xCa cluster[1] of the WOC suggests that the dynamics of proton shifts within the network of hydrogen bonds also affect the mechanism of the redox reactions within the WOC with respect to the coupling between ET and PT steps (for former discussions on this topic, see [44,45]).

It is obvious that the absence of the Mn_4O_xCa cluster significantly modifies the reaction coordinate of $P680^{+\cdot}$ reduction by Y_z. In PS II complexes deprived of the WOC the "fast ns" kinetics completely disappear and the overall reaction is dominated by pH dependent μs kinetics [46–49]. This process is characterized by a markedly larger activation energy (factor of about 3) and a significant KIE of 2.7–3.0 (for a review, see [50]). Furthermore, the reaction is coupled with a stoichiometric proton release into the outer aqueous bulk phase [51].

Values of 1.6 ± 0.2 eV and 11 ± 1 Å are obtained for reorganization energy and edge-to-edge distance between $P680^{+\cdot}$ and Y_z, respectively, when analyzing the kinetic data by using Eqs. (1)–(3). Interestingly, the magnitude of the reorganization energy in the samples lacking an intact WOC is significantly larger than in PS II preparations containing the WOC and closely resembles the number of 1.4 eV reported for model systems in solution [52]. This finding reflects a drastic change of the microenvironment of Y_z when the Mn_4O_xCa cluster of the WOC is lacking, whereas the distance to $P680^{+\cdot}$ is expected to remain virtually invariant. A slight enlargement of the distance (by about 1 Å) calculated on the basis of Eqs. (2) and (3) might therefore indicate that the reaction rate is not entirely limited by the rate of nonadiabatic electron transfer but also affected by the proton transfer. This idea is in line with a recent detailed analysis on Mn-depleted PS II core complexes isolated from mutants of cyanobacteria where the ΔG^0 value of Y_Z oxidation by $P680^{+\bullet}$ was varied due to modulation of the reduction potential of P680 ($\Delta E \sim 80$ mV) and also the pK_a of Y_Z was changed through replacement of Tyr by the 3-fluoro-Tyr ($\Delta pK_a \sim 1.5$). A switch of the reaction mechanism was deduced from this data: at pH<7.5 a concerted PCET takes place while at pH>7.5 a sequential PT/ET process occurs [53].

Based on these findings and considerations on the hydrogen bond network and its functional relevance it is clear that sound conclusions on the reaction coordinate of Y_z oxidation in PS II complexes with a functionally competent water oxidation to O_2 cannot be drawn by using data gathered from samples with a destroyed WOC (see also [50]). The most important conclusion of the present analysis is the rate limitation of the redox step by nonadiabatic electron transfer in samples with an intact WOC. In the following oxidized Y_z will be symbolized by Y_z^{ox} rather than by $Y_z^{\cdot}$ in order to keep in mind the unknown transient location of the proton released.

[1] The 1.9 Å XRDC structure [26] clearly shows a Mn_4O_5Ca cluster. In order to keep in mind the possibility that the number of oxo-bridges could change in S_3 and S_4 the index x is used instead of 5 throughout this paper.

3.2. Stepwise oxidation of the WOC by Y_z^{ox}

The kinetics of Y_z^{ox} induced oxidation steps in the WOC [37,54–56], their dependencies on temperature [37,57,58] and on replacement of exchangeable protons by deuterons [37,59–61] have been thoroughly studied. A collection of representative data is compiled in Table 1.

When rate constants and activation energies for the redox steps $Y_z^{ox}S_i \rightarrow Y_zS_{i+1} + n_iH^+$ of spinach PS II membrane fragments for i = 0, 1 and 2 (see Table 1) are analyzed within the framework of Eqs. (2)–(3), analogous to that performed for $P680^{+\cdot}$ reduction by Y_z (see former section), values of about 16 ± 1 Å and 12 ± 1 Å are obtained for the edge-to-edge distance between Y_z^{ox} and the redox active manganese in states S_1 and S_2, respectively (the value for WOC oxidation $Y_z^{ox}S_0 \rightarrow Y_zS_1 + n_0H^+$ is about 18 ± 3 Å but this number is less precise due to limited kinetic information, vide infra). Regardless of the uncertainties of these numbers the calculated values are in drastic contrast to the distances gathered from XRDC structure data where the longest edge-to-edge distance was found to be 8.04 Å [18]. This discrepancy unambiguously shows that the rate of all oxidation steps in the WOC driven by Y_z^{ox} is definitely not limited by non-adiabatic electron transfer but by trigger reaction(s).

In order to analyze this crucial point in more detail, rate constants for nonadiabatic electron transfer $k_{i+1,i}^{NET}$ were calculated by using Eqs. (2)–(3) and compared with experimental data obtained for PS II membrane fragments. In all cases the longest distance of 8.04 Å was used because at shorter distances the $k_{i+1,i}^{NET}$ values are even larger. The results obtained are compiled in Table 2. Inspection of this data readily shows that the "theoretical" rate constants $k_{i+1,i}^{NET}$ are larger by several orders of magnitude than the experimental data. This tremendous difference unambiguously reveals that the redox steps $Y_z^{ox}S_i \rightarrow Y_zS_{i+1} + n_iH^+$ are triggered reactions for i = 0, 1 and 2 (the reaction $Y_z^{ox}S_3 \rightarrow \rightarrow \rightarrow Y_zS_0 + O_2 + n_3H^+$ will be discussed separately).

As a consequence, each redox step of the WOC for i = 0, 1 and 2 has to be described by a sequential reaction of the type:

$$Y_z^{ox}S_i \xrightarrow{k_{i^*,i}^{trigg}} (Y_z^{ox}S_i)^* \xrightarrow{k_{i+1,i}^{NET}} Y_zS_{i+1} + n_iH^+ \quad (4)$$

where $k_{i^*,i}^{trigg}$ is the rate constant of the triggering process in redox state S_i which precedes the electron transfer step and is rate limiting for the overall reaction, i.e. $k_{i^*,i}^{trigg} \ll k_{i+1,i}^{NET}$, and $(Y_z^{ox}S_i)^*$ represents a "triggered" redox state S_i.

The sequence (4) necessarily implies that all redox transitions of the WOC are characterized by a sigmoidial time course. Accordingly the deviation from a pure mono-exponential kinetics should provide information on the rate of the redox step. However, this feature could not be resolved due to limitations of the applied methods and in particular because the effect is extremely small for $k_{i^*,i}^{trigg} \ll k_{i+1,i}^{NET}$ and therefore it remains buried by the error margins originating from the signal/noise ratios. Regardless of this problem, an important mechanistic consequence emerges from Eq. (4) and the relation $k_{i^*,i}^{trigg} \ll k_{i+1,i}^{NET}$: the experimentally obtained activation energies reflect the temperature dependence of the trigger reaction(s) rather than the characteristics of the redox step in the physiological range. Likewise, the transient population of the triggered redox states $(Y_z^{ox}S_i)^*$ is extremely small and therefore escapes an experimental characterization.

As a consequence of the conclusions on the existence of trigger processes, the Kok scheme has to be extended as is shown in Fig. 5. The redox states S_i in the triggered conformation are symbolized by stars. The exact pathway of proton release is not known and expected to be S_i state dependent. Therefore Fig. 5 can only present a schematic description of this topic without specifying whether proton release is correlated with the formation of the triggered state $(Y_z^{ox}S_i)^*$ or with the electron transfer step.

A very important property of the transitions into $(Y_z^{ox}S_i)^*$ is the thermal blockage below threshold temperatures. This striking feature indicates that at least one breakpoint exists in the reaction coordinate of the triggering process. Table 2 presents data of the characteristic temperatures for 50% inhibition (δ_c) of the S_i state transitions in PS II membrane fragments [62]. Markedly higher values of δ_c ($\Delta\delta_c$ = 30 to 50 K) were found for PS II core complexes from *T. vulcanus* [63]. Data on PS II core complexes from spinach are described in [64]. It is most interesting to note that an analogous phenomenon of freezing has also been observed for the electron transfer from $Q_A^{-\cdot}$ to Q_B at the acceptor side of PS II [65–68]. This effect was shown to be strictly correlated with protein dynamics [69,70]. In Fig. 6 the range of thermal blockage of the S_i state transitions is compared with the temperature dependence of both the electron transfer from $Q_A^{-\cdot}$ to Q_B and the protein flexibility. Inspection of this data reveals that the Y_z^{ox} induced trigger reactions of the WOC in redox states S_0, S_2 and S_3 exhibit a similar dependence on the overall protein dynamics of the PS II core as the $Q_A^{-\cdot}$ reoxidation by Q_B while the reaction of S_1 becomes blocked in a range of markedly lower environmental mobility. In addition to freezing also dehydration of the samples below thresholds of relative humidity leads to inhibition of both $Q_A^{-\cdot}$ reoxidation by Q_B [71] and S_i state transitions by Y_z^{ox} [72].

The mechanism of the triggering reactions has been neither resolved for the acceptor nor for the donor side of PS II. However, in case of the triggered oxidation of $Q_A^{-\cdot}$ by Q_B it is possible to separate kinetically the trigger reaction from the electron transfer step because the distance between the two redox groups is about 13 Å (17) so that k^{NET} is of the same order of magnitude as k^{exp}. Indeed, evidence has been presented for a transition from bi- to mono-dentate coordination of the bicarbonate ligand to the non-heme iron [73] thus supporting the idea of a structural rearrangement giving rise to the triggered state. Furthermore, proton transfer step(s) are most likely to be involved in triggering. A role of proton shift(s) in gating the redox reactions of the WOC is in line with the markedly lower threshold temperature of the $S_1 \rightarrow S_2$ transition compared to the redox steps of the other S_i state transitions (see Table 2 and Fig. 6) because the latter reactions are, but the former reaction is not, coupled with significant proton release into the lumen [74]. When taking into account this argument, the trigger reactions are likely to be similar for i = 0 and i = 2, but different for i = 1. Accordingly, the value of 250 μs for

Table 1
Half life times $t_{1/2}$ (μs) of the reactions $Y_Z^{OX}S_i \rightarrow Y_ZS_{i+1-4\delta_{i3}} + \delta_{i3}O_2 + n_iH^+$ (δ_{i3} = 1 for i = 3, otherwise zero) in PS II core complexes from *Thermosynechococcus* (*T.*) *vulcanus* at 25 °C and in PS II membrane fragments (PS II m.f) and PS II core complexes from *spinacea oleracea* at 20 °C and corresponding activation energies E_A (kJ/mol) of the different samples.

Species	*Spinacela oleracea*				*T. vulcanus*	
Preparation	PSII m.f. [58]		PSII core [37]		PSII core [57]	
	$t_{1/2}$	E_A	$t_{1/2}$	E_A	$t_{1/2}$	E_A
i = 0	50	5	n.d	n.d	n.d.	n.d.
i = 1	100	12.0	75	14.8	70	9.6
i = 2	220	36.0	225	35.0	~130	26.8
i = 3	1300	20/46[a]	4100	21/67[a]	1300	~16/60[a]

[a] Values below/above threshold temperature (for details, see text).

Table 2
Calculated rate constants of non-adiabatic electron transfer $k_{i+1,i}^{NET}$ (s^{-1}) and experimental rate constants $k_{i+1,i}^{exp}$ (s^{-1}) and kinetic isotope (H/D) effects at 20 °C, activation energies E_A (kJ/mol), and threshold temperatures of 50 % blockage $\delta_{1/2}$ (K) of the reactions $Y_Z^{OX}S_i \rightarrow Y_ZS_{i+1-4\delta_{i3}} + \delta_{i3}O_2 + n_iH^+$ (δ_{i3} = 1 for i = 3, otherwise zero) in PS II membrane fragments from *spinacea oleracea*.

i	$k_{i+1,i}^{NET}$	$k_{i+1,i}^{exp}$ [58]	$E_{A,i+1,i}$ [58]	$\delta_{1/2}$, [62]	k_H/k_D[37]
0	$>10^9$	$1.4\ (0.3) \cdot 10^4$	5	223	n.d.
1	$\approx 10^9$	$7 \cdot 10^3$	12.0	138	1.3
2	$\approx 10^9$	$3.3 \cdot 10^3$	36.0	228	1.3
3	$\approx 10^6$	$5 \cdot 10^2$	20.0 (46.0)[a]	233	1.4

[a] Values below/above threshold temperature (for details, see text).

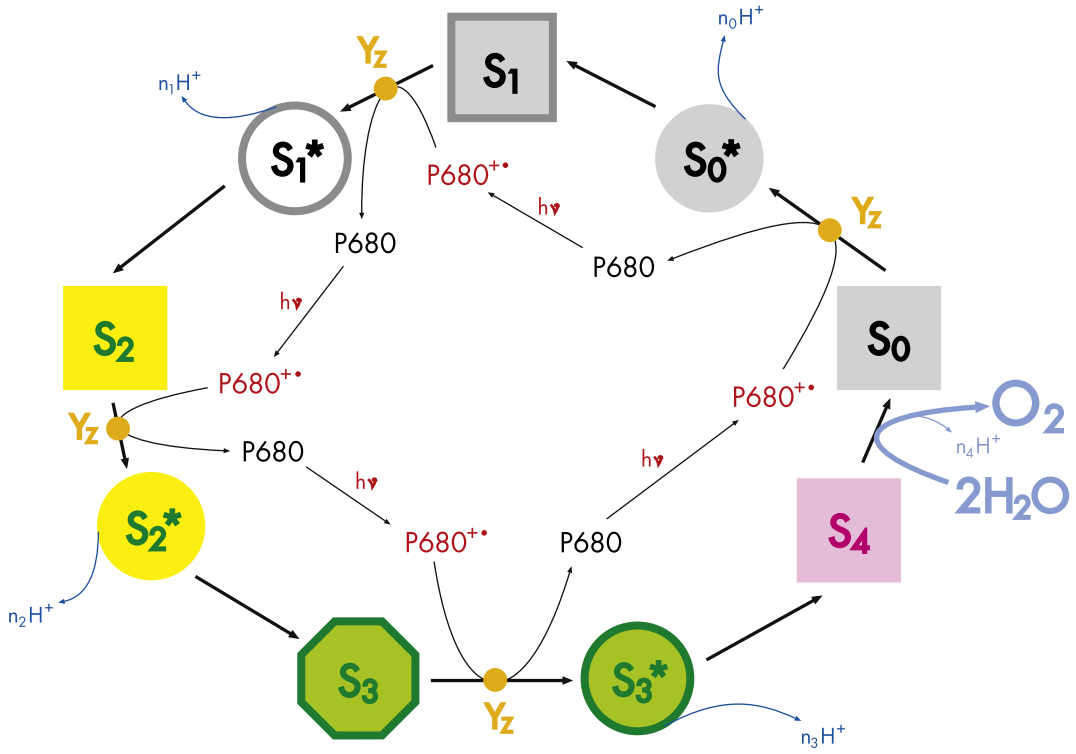

Fig. 5. Extended Kok cycle of oxidative water splitting driven by $P680^{+\cdot}$ with Y_z acting as intermediate and the S_i states in their transient triggered conformation (symbolized by a star). For the sake of simplicity the "super-reduced" S_{-i} states are omitted because they are not involved in the process of water oxidation. For further details, see text.

the $S_0 \rightarrow S_1$ transition [56] appears to be more realistic than the number of 30 μs [55].

3.3. Reaction sequence of Y_z^{ox} reduction by the WOC in redox state S_3 leading to O_2 formation and release

In contrast to the apparent mono-exponential kinetics (vide supra) reflecting the rate limiting triggering reactions for i = 0, 1 and 2, the time course of Y_z^{ox} reduction by the WOC in redox state S_3 is sigmoidal and the overall rate is significantly slower and more variable (for further details, see [75] and references therein). This reaction can be basically described by the following simplified sequence:

$$Y_z^{ox}S_3 \xrightarrow{k^{trigg}_{3*,3}} (Y_z^{ox}S_3)^* \xrightarrow{k_{4,3}} Y_z[S_2(H_xO_2)^c] \xrightarrow{k_{0,4}} Y_z[S_0(O_2)^c] + n_3H^+ \quad (5)$$

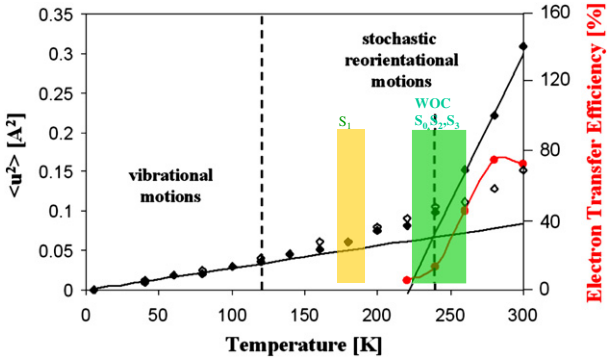

Fig. 6. Temperature dependence of the average atomic mean square displacement $<u^2>$ for hydrated (full symbols) and dry PS II membrane fragments (open symbols). The temperature ranges of different mobility characteristics are separated by dashed lines. The thermal blockage of S_1 oxidation and S_0, S_2 and S_3 reactions are marked by areas in yellow and green, respectively.

where $[S_2(H_xO_2)^c]$ and $[S_0(O_2)^c]$ reflect complexed (symbol c) peroxide and molecular dioxygen of unresolved mode of ligation, respectively, x symbolizes the unknown protonation state of complexed peroxide and n_3 the overall H^+ release without specifying the individual step(s) of deprotonation. For the sake of simplicity, intermediates between $(Y_z^{ox}S_3)^*$ and $Y_z[S_2(H_xO_2)^c]$ as well as the last strongly exergonic step of the product (O_2) exchange by substrate water [13,76] are omitted and back reactions are not explicitly shown.

Two different types of rate limitation of sequence (5) can be considered: i) the triggering process is slow compared to the redox reaction(s) and comprises a sequence of at least two steps with different kinetics thus giving rise to the sigmoidal time course, or ii) a single triggering reaction with similar kinetics as those of the other S_i state transitions is followed by an overall electron transfer which is markedly slower due to participation of a fast uphill redox equilibrium of the type $L \underset{k_{LH}}{\overset{k_{HL}}{\rightleftharpoons}} H$ (L = low energy and H = high energy state) which is characterized by a rather small apparent constant $K^{eq}_{HL} = k_{HL}/k_{LH} \ll 1$.

At present there exists no experimental evidence for a sequence of trigger reactions with different kinetics. The second alternative appears to be more attractive and therefore will be analyzed in greater detail. The key point of the mechanism of reaction sequence (5) is the nature of the WOC in the triggered redox state $(Y_z^{ox}S_3)^*$. At first it must be emphasized that electronic configuration and nuclear geometry of redox state S_3 are not yet unambiguously clarified. Even a fundamental problem for all S_i states is still a matter of current debate, i.e. the overall valence state of the manganese cluster (for a review, see [77]). At present $Mn(III)Mn(IV)_3$ is the widely accepted electronic configuration of S_2 (see [78–80] and references therein) with corresponding ramifications to the other S_i states ("high valence manganese" model). However the alternative of $Mn(III)_3Mn(IV)$ for S_2 ("low valence manganese" model) cannot be entirely ruled out (for a discussion, see [81]). An unambiguous clarification of this topic is an indispensable prerequisite for all detailed theoretical studies on the mechanism of the redox steps but

it does not affect the following considerations on the mode of reaction sequence (5).

Apart from the exact overall valence state of the four manganese (vide supra) two basically different types of models of S_3 are currently under discussion (for details, see [2,77,78] and references therein): (a) S_3 is a single state with an electronic configuration that is characterized either by a manganese which is oxidized compared to S_2 (referred to as "Mn-only" model A) or by electron abstraction from an oxygen atom thus giving rise to formation of an oxo-radical in the Mn_4O_xCa cluster which remains at virtually the same total manganese oxidation level as in S_2 ("Oxo-radical" model B), and (b) S_3 is a multiple state comprising different forms which are interchangeable via rapid redox isomerism and tautomerism equilibria ("multiple S_3 state" model C). It is now widely accepted that the linkage of the two oxygen

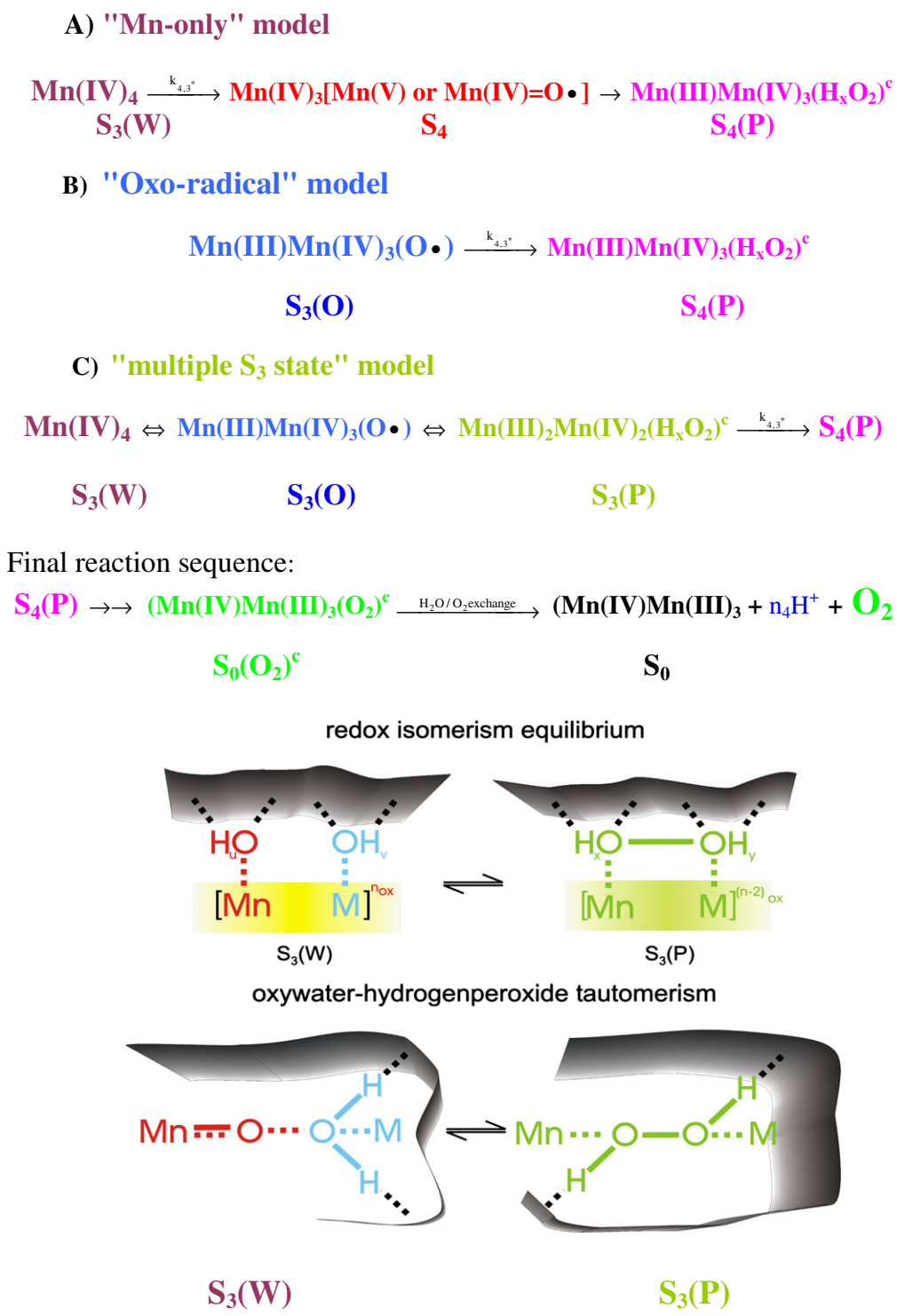

Fig. 7. Schematic representation of the "Mn only" model A, the "Oxo" model B and the "S_3 multistate" model C (top panel) and the redox isomerism equilibrium and proton tautomerism (bottom panel).In the upper panel the different possible electronic configurations of the S_3 state and the corresponding names of model A and B are printed in margenta and blue, respectively, the name of model C is presented in the same color as the presumed peroxidic configuration $S_3(P)$. The final reaction sequence following formation of $S_4(P)$ is assumed to be the same in all models. It must be emphasized that the manganese valence state presented corresponds with the widely accepted "high valence manganese" model (for details, see text).

atoms occurs at the substrate redox level of a complexed peroxide as previously proposed [13] but the details of the process remain to be clarified (vide infra). Based on the proposed nature of S_3 the two alternatives (a) and (b) fundamentally differ in the redox state of the WOC where the essential O–O bond can be formed.

The top panel of Fig. 7 illustrates the reaction sequences of models A, B and C using the conventional concept of the "high valence manganese" configuration (vide supra).

In type (a) models (A and B) the extraction of an electron from the WOC in redox state S_3 by Y_z^{ox} is assumed to be the prerequisite for the covalent linkage of the two substrate oxygen atoms forming the complexed peroxide (for different models, see [82–90]). At present this idea is the widely accepted paradigm ("S_4 dogma"). An endergonic reaction $(Y_z^{ox}S_3)^* \underset{k^{redox}_{3^*,4}}{\overset{k^{redox}_{4,3^*}}{\rightleftharpoons}} Y_z[S_2(H_xO_2)^c] = Y_zS_4(P)$ with a rather small apparent equilibrium constant $K^{eq}_{4,3^*}$ (vide supra) is inferred to determine the rate of the slow overall Y_z^{ox} reduction where $S_4(P)$ symbolizes the complexed peroxide in redox state S_4 (for the sake of simplification intermediary states like the postulated $Mn(IV)=O^{\cdot}$ radical will be omitted in the kinetic simulations). The assumption of an uphill reduction of Y_z^{ox} by the WOC in S_3 is in line with calculations based on functional density theory (DFT) [83,84]. It is worth mentioning that the proposal of an "energy rich" intermediate is also integral part of the "multiple S_3 state" model (vide infra).

This model as an alternative to the "S_4 dogma" is based on the original idea that in the WOC a state can be populated at the redox level of S_3 which attains the electronic configuration and nuclear geometry corresponding with a complexed peroxide [13]. It was postulated (see [91] and references therein) that this peroxidic state of the WOC is one form of redox isomerism and proton tautomerism with rapid equilibration rates:

$$S_3(W) \underset{k_{WO}}{\overset{k_{OW}}{\rightleftharpoons}} S_3(O) \underset{k_{OP}}{\overset{k_{PO}}{\rightleftharpoons}} S_3(P) \qquad (6)$$

where the different S_3 states symbolized by $S_3(W)$, $S_3(O)$ and $S_3(P)$ reflect formal oxidation levels of the substrate where W = water, O = bound oxo-radical and P = complexed peroxide.

The top panel of Fig. 7 schematically summarizes the models A, B and C. Within the framework of the "high valence manganese" concept $S(W)=Mn(IV)_4$, $S_3(O)=Mn(III)Mn(IV)_3(O^{\cdot})$ and $S_3(P)=Mn(III)_2Mn(IV)_2(H_xO_2)^c$ where $H_xO_2)^c$ is a complexed peroxidic state of unknown protonation x. The bottom panel shows a simplified scheme of redox isomerism and proton tautomerism comprising only states $S_3(W)$ and $S_3(P)$.

The peroxidic state $S_3(P)$ is assumed to be: i) the "entatic state" for the reduction of Y_z^{ox} under concomitant formation of the generally accepted complexed peroxidic form $S_4(P)=[S_2(H_xO_2)^c]$, and ii) populated with low probability, due to its higher energy level compared to $S_3(W)$ and $S_3(O)$. This model which has been discussed in detail in recent reviews [2,77,91] implies that the rate constant of Y_z^{ox} reduction by the WOC at redox level S_3 depends critically on the population probability of the peroxidic state $S_3(P)$.

3.4. Simulation of the time course of Y_z^{ox} reduction by the WOC in redox state S_3 leading to O_2 formation and release

For further considerations on the mode of S_3 oxidation by Y_z^{ox}, kinetic analyses were performed on the basis of models A, B and C. Fig. 8 presents simplified reaction patterns of these models. The final reaction sequence leading from the complexed peroxidic intermediate $S_4(P)$ to the release of O_2 and proton(s) (see Fig. 7) are summarized by an overall rate constant k_{O_2}. In case of the "multiple S_3 state" model C the redox step giving rise to Y_z^{ox} reduction by the WOC is assumed to comprise only the entatic state $S_3(P)$ (vide supra). Furthermore, in order to avoid too many parameters, the evaluation is simplified by replacing the equilibrium (6) by $[S_3(W) \underset{k_{WP}}{\overset{k_{PW}}{\rightleftharpoons}} S_3(P)]$ and $[S_3(W) \underset{k^*_{WP}}{\overset{k^*_{PW}}{\rightleftharpoons}} S_3(P)]^*$.

The numerical fits were based on three characteristic features of the experimental findings: i) appearance of a lag phase [37,54–56,92,93], ii) virtually synchronous time course of Y_z^{ox} reduction by the WOC in redox state S_3 and of O_2 release [93–95], and iii) variability of the overall rate depending on different parameters [37,57,96–99].

The striking similarity of the characteristic temperatures of thermal blockage (except of S_1 oxidation, see Table 2) suggests that the rate constant $k^{trigger}_{3^*,3}$ of the trigger reaction is of comparable magnitude to $k^{trigger}_{i^*,i}$ of the S_i state transitions (i = 0, 1 and 2) and therefore the value of $k^{trigger}_{3^*,3}$ is assumed to be in the range of 10^3–$10^4\ s^{-1}$ (see Table 2). This idea is used in the numerical fit of all models (see legend of Fig. 9).

The panels on the left side of Fig.9 show for the time course of Y_z^{ox} reduction and O_2 release typical simulation curves obtained within the framework of the models based on the "S_4 dogma" (A and B are the same in this analysis). A satisfying fit is achieved with reasonable assumptions on the rate constants. Interestingly, the absolute values of the rate constants $k^{redox}_{4,3^*}$ and $k^{redox}_{3^*,4}$ can be varied within several orders of magnitude without marked effects provided that an appropriate ratio $k^{redox}_{4,3^*}/k^{redox}_{3^*,4}$ is used (data not shown). A significant decrease of this ratio by a factor of about 10 leads to a marked retardation of the overall kinetics (compare Fig. 9A and B). This result illustrates

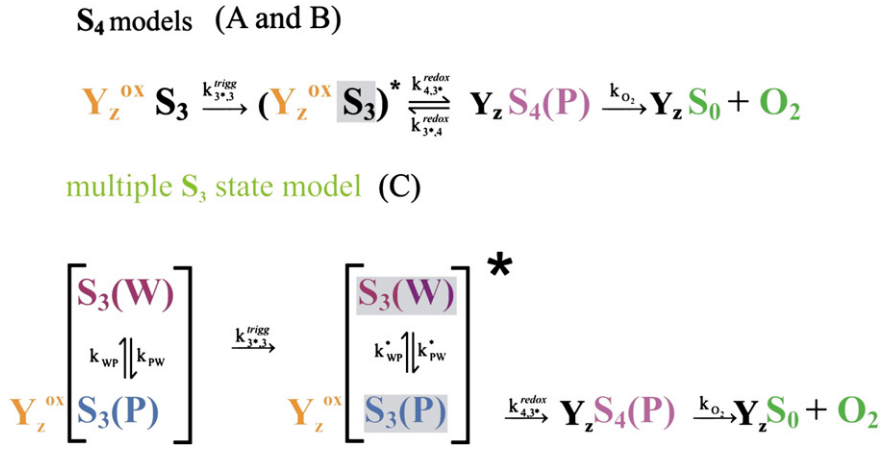

Fig. 8. Simplified schemes of "S_4 models" (top) and "S_3 multistate" model (bottom). For details, see text.

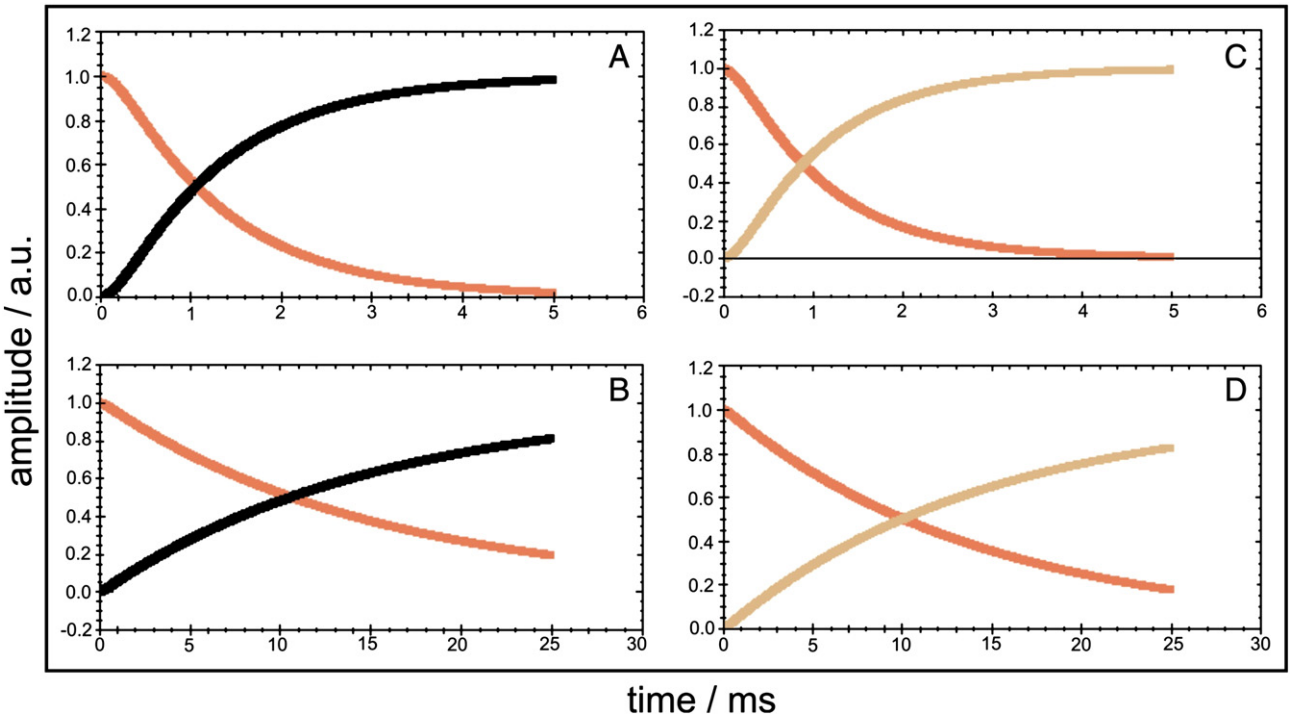

Fig. 9. Simulated kinetics of Y_z^{ox} reduction (red lined curves) and O_2 release(black lined curves in panels A and B, ochre lined curves in panels C and D) within the framework of "S_4 models" (left side panels) and of the "S_3 multistate" model (right side panels). The following rate constants were used: $k_{3^*,3}^{trigger} = 5 \cdot 10^3\ s^{-1}$, $k_{4,3^*}^{redox} = 10^3\ s^{-1}$, $k_{3^*,4}^{redox} = 10^4\ s^{-1}$, $k_{O_2} = 5 \cdot 10^4\ s^{-1}$ (panel A); $k_{3^*,3}^{trigger} = 5 \cdot 10^3\ s^{-1}$, $k_{4,3^*}^{redox} = 10^3\ s^{-1}$, $k_{3^*,4}^{redox} = 7 \cdot 10^5\ s^{-1}$,$k_{O_2} = 5 \cdot 10^4\ s^{-1}$ (panel B); p = 0.02, $k_{3^*,3}^{trigger} = 5 \cdot 10^3\ s^{-1}$, $k_{PW}{}^* = 10^3\ s^{-1}$, $k_{WP}{}^* = 10^4\ s^{-1}$, $k_{4,3^*}^{redox} = 10^8\ s^{-1}$and $k_{O_2} = 5 \cdot 10^4\ s^{-1}$ (panel C); and p = 0.002, $k_{3^*,3}^{trigger} = 5 \cdot 10^3\ s^{-1}$, $k_{PW}{}^* = 70\ s^{-1}$, $k_{WP}{}^* = 10^4\ s^{-1}$, $k_{4,3^*}^{redox} = 10^8\ s^{-1}$and $k_{O_2} = 5 \cdot 10^4\ s^{-1}$ (panel D).

the key effect of the "uphill" $S_4(P)$ formation (see former section) on the experimentally detected rates of Y_z^{ox} reduction and O_2 release.

Analogous simulations within the framework of the "multiple S_3 state" model comprise population probabilities $(1-p)$ and p of forms $S_3(W)$ and $S_3(P)$, respectively, in the equilibrium $[S_3(W) \underset{k_{WP}}{\overset{k_{PW}}{\rightleftharpoons}} S_3(P)]$ as variable fit parameter. Typical simulation curves are shown on the right side of Fig. 9. Each individual rate constant and p were varied by keeping the other parameters constant in order to check their limits in describing the experimental data. This mode of analysis revealed: i) a value of 0.05 is the upper limit of parameter p, i.e. the population probability of $S_3(P)$ has to be <5% and – if form $S_3(P)$ really exists – it is therefore expected to be very difficult to detect experimentally (the transient population of $S_3(P)^*$ in the triggered state is even much lower ($<10^{-5}$) due to its rapid oxidation by Y_z^{ox}), ii) rate constant $k_{PW}{}^*$ significantly affects the overall time course of Y_z^{ox} reduction and O_2 release (compare Figs. 9C and 9D), i.e. their experimentally observed variability [96–99] are explained by a change of $k_{PW}{}^*$, iii) rate constants $k_{WP}{}^*$ and $k_{4,3^*}^{redox}$ can be varied over wide ranges ($10^3 \ldots 10^5\ s^{-1}$ and $10^5 \ldots 10^8\ s^{-1}$, respectively), and iv) k_{O_2} has a lower limit of about $4 \cdot 10^3\ s^{-1}$, i.e. the reactions following the 1-electron transfer from the WOC in S_3 to Y_z^{ox} have to be comparatively fast. The same feature of k_{O_2} is also obtained for simulations using the "S_4 dogma" models (see Fig. 9, left panels).

4. Concluding remarks

The present analyses reveal that Y_z oxidation by $P680^{+\cdot}$ in samples with intact WOC is kinetically limited by non-adiabatic electron transfer and its extent thermodynamically determined by relaxation processes of the environment. In marked contrast, the oxidation steps of the catalytic site in the WOC up to redox level S_3 are kinetically limited by triggering processes which are slower by orders of magnitude than non-adiabatic electron transfer and become thermally blocked below characteristic threshold temperatures. The simulation studies showed that experimental findings on the kinetic characteristics of Y_z^{ox} reduction by the WOC in redox state S_3 and of O_2 release [37,54–57,92–99] are well described by the two different types (a and b) of models discussed above. Moreover, the experimental data can be properly simulated by different sets of rate constants for the forward and backward redox steps. Therefore, this type of analysis cannot offer a discrimination between these models.

An essential postulate of the "multiple S_3 state" model is the general idea that the redox states S_i per se are not characterized by a single electronic configuration and nuclear geometry but comprise different forms (see [91,100] and references therein). The assumption on the existence of multiple S_i states is supported by theoretical calculations leading to the conclusion that already the dark stable redox state S_1 comprises two isomeric forms which are in thermal equilibrium [101]. Likewise, the S_2 state is known to populate two states with different magnetic properties at low temperatures [102–105] and also the $S_2Y_z^{ox}$ split signals are indicative of two different forms (see [106,107] and references therein).

At present direct experimental evidence is lacking for the existence of the presumed multiple state equilibrium (6) in redox state S_3. However, there are some indirect lines of evidence for different forms of redox state S_3. Studies on the S_3 state properties via analysis of the $S_2Y_z^{ox}$ split signal at low temperatures are indicative of two different S_3 forms [107]. The pronounced heterogeneity of several mutants with respect to the extent of oxygen evolution capacity (for a review, see [108]) could reflect a multistate model because inhibition in populating the "entatic" state $S_3(P)$ in a fraction of the WOCs in these mutants is expected to give rise to blockage of Y_z^{ox} reduction by S_3 and consequently of diminished O_2 evolution of the whole ensemble of PS II complexes. Of particular interest is the CP43-E354 mutant of *Synecocystis* sp. PCC 6803 [109,110]. The replacement of Glu by Gln at site 354 of CP43 could interrupt in a large fraction of the PS II complexes the proton shift(s) that is (are) required for population of the $S_3(P)$ form. These modified

complexes are unable to evolve O_2 because oxidation of S_3 by Y_z^{ox} is blocked due to lack of the entatic state S_3(P) of the reaction. In other cases a perturbation of the hydrogen bond network could give rise to a retardation of Y_z^{ox} reduction by S_3 rather than to cause blockage. This type of modification has been shown to arise in samples where the Ca^{2+} of the Mn_4O_xCa cluster is replaced by Sr^{2+}[111]. The Ca^{2+}/Sr^{2+} exchange was shown to perturb the distribution of conformational microstates of S_3 thus retarding the reaction [112]. In mutants both effects can arise simultaneously, i.e. a fraction of the PS II complexes is completely blocked while in another fraction only the kinetics are retarded.

The role of protons is not only restricted to its proposed key function in O–O bond formation but appears also to be of relevance for reactivity and stability of redox states S_2 and S_3. Lipophilic protonophores are known to significantly affect the properties of both S_2 and S_3 thus leading to reversible "turning off and on" oxygen evolution by variation of either the frequency of repetitive single turnover flash excitation [113] or of the actinic CW light intensity (unpublished data). This effect referred to as ADRY effect [113] was ascribed to a decrease of the life time of S_2 and S_3[114–116]. On the other hand, a drastic lengthening of the lifetime of S_2 and a blockage of the $S_2 \rightarrow S_3$ transition was observed upon depletion of chloride [117–120] which is shown to be part of hydrogen bonding in the vicinity of the Mn_4O_xCa cluster [18,26]. Therefore it appears to be most important to gather further information on the mechanistic role of protons and hydrogen bond networks in determining the properties of S_2 and S_3 and of oxidative water splitting, Suitable experimental and theoretical approaches are required to address this topic. Among these FTIR difference spectroscopy in combination with isotope labeling and site directed mutagenesis appears to be a most promising tool in obtaining new information as outlined in recent reports [121,122].

Based on former considerations [100] and currently available information on hydrogen bond network(s) and bound water molecules [18,26], the protein matrix of the WOC including bound water molecules is postulated to play an active role in providing a specially tuned dynamic landscape of a scalar proton field with local gradients that are essential for the O–O bond formation [2,100]. In this way the WOC acts as a molecular nano-scale machine (for former discussion, see [123]). This mode of sophisticated catalysis is most likely responsible for the high efficiency and turnover rate which exceeds that of currently available biomimetic catalysts with comparable Mn_yO_xCa motifs by orders of magnitude (see [124] and references therein). As the dynamics of the proton landscape in the environment of the Mn_yO_xCa cluster become functionally blocked below characteristic thresholds of temperature and protein hydration levels, questions arise as to what extent detailed information on the characterization of the WOC at very low temperatures, where the formation of the indispensable triggered states is definitely prevented, can really be extrapolated to understand the mechanism of oxidative water splitting at work (for an earlier discussion. see [125]).

Note added in proof

After submission of the revised manuscript I became aware of new seminal work on quantum chemical calculations analyzing the mechanism of oxidative water splitting on the basis of the 1.9 Å XRDC structure of PS II [126]. This study provides theoretical support for the possibility to populate a peroxidic state in S_3 which is a basic postulate of the "multiple S_3 state" model.

Acknowledgements

I am very grateful to Marco Vitali for providing the computer program for kinetic simulations and to J.-R. Shen for the structure data used for Fig. 4. I also would like to thank for preparing electronic versions of the figures: Jan Kern (Fig. 1), Susanne Renger (Figs. 2 and 5), Philipp Kühn (Fig. 3), Christoph Theiss (Figs. 2, 4 and 9), Jörg Pieper (Fig. 6), Ronald Steffen (Fig. 7) and Franz Josef Schmitt (Fig. 8). The highly competent evaluation by anonymous reviewers and financial support by Deutsche Forschungsgemeinschaft (Sfb 429) and Bundesminisaterium für Forschung und Technologie (RUS 11/014) are gratefully acknowledged.

References

[1] G. Renger, B. Ludwig, Mechanism of photosynthetic production and respiratory reduction of molecular dioxygen: a biophysical and biochemical comparison, in: G. Peschek, C. Obinger, G. Renger (Eds.), Bioenergetic Processes of Cyanobacteria — From Evolutionary Singularity to Ecological Diversity, Springer, Dordrecht, The Netherlands, 2011, pp. 337–394.
[2] G. Renger, T. Renger, Photosystem II, the machinery of photosynthetic water splitting, Photosynth. Res. 98 (2008) 53–81.
[3] L.-X. Shi, W.P. Schröder, The low molecular mass subunits of the photosynthetic supracomplex, photosystem II, Biochim. Biophys. Acta 1608 (2004) 75–96.
[4] L.-X. Shi, M. Hall, C. Funk, W.P. Schröder, Photosystem II, a growing complex: updates on newly discovered components and low molecular mass proteins, Biochim. Biophys. Acta 1817 (2012) 13–25.
[5] J. Raymond, R.E. Blankenship, The evolutionary development of the protein complement of Photosystem 2, Biochim. Biophys. Acta 1655 (2004) 133–139.
[6] W. Lubitz, E.J. Reijerse, J. Messinger, Solar water-splitting into H_2 and O_2: design principles of photosystem II and hydrogenases, Energy Environ. Sci. 1 (2008) 15–31.
[7] D.G. Nocera, Chemistry of personalized solar energy, Inorg. Chem. 48 (21) (2009) 10001–10017.
[8] V. Petrouleas, A.R. Crofts, The iron–quinone acceptor complex, in: T. Wydrzynski, K. Satoh (Eds.), Advances in Photosynthesis and Respiration, Volume 22, Springer, Dordrecht, 2005, pp. 177–206.
[9] J. Kern, G. Renger, Photosystem II: structure and mechanism of the water:plastoquinone-oxido:reductase, Photosynth. Res. 94 (2007) 183–202.
[10] W.W. Parson, Functional patterns of reaction centers in anoxygenic photosynthetic bacteria, in: G. Renger (Ed.), Primary Processes of Photosynthesis: Priniciples and Apparatus, Part II Reaction Centers/Photosystems, Electron Transport Chains, Photophosphorylation and Evolution, Royal Society Chemistry, Cambridge, 2008, pp. 57–109.
[11] R. Lancaster, Structures of reaction centers in anoxygenic bacteria, in: G. Renger (Ed.), Primary Processes of Photosynthesis: Priniciples and Apparatus, Part II: Reaction Centers/Photosystems, Electron Transport Chains, Photophosphorylation and Evolution, Royal Society Chemistry, Cambridge, 2008, pp. 5–56.
[12] A.B. Anderson, T.V. Albu, Ab initio determination of reversible potentials and activation energies for outer-sphere oxygen reduction to water and the reverse oxidation reaction, J. Am. Chem. Soc. 121 (1999) 11855–11863.
[13] G. Renger, Theoretical studies about the functional and structural organization of the photosynthetic oxygen evolution, in: H. Metzner (Ed.), Photosynthetic Oxygen Evolution, Academic Press, London, 1978, pp. 229–248.
[14] G. Renger, Water cleavage by solar-radiation — an inspiring challenge of photosynthesis research, Photosynth. Res. 38 (1993) 229–247.
[15] R.J. Debus, B.A. Barry, I. Sithole, G.T. Babcock, L. McIntosh, Directed mutagenesis indicates that the donor to $P680^+$ in photosystem II is tyrosine-161 of the D1 polypeptide, Biochemistry 27 (1988) 9071–9074.
[16] J.G. Metz, P.J. Nixon, M. Rögner, G.W. Brudvig, B.A. Diner, Directed alteration of the D1 polypeptide of Photosystem II: evidence that tyrosine 161 is the redox component, Z, connecting the oxygen-evolving complex to the primary electron donor, P680, Biochemistry 28 (1989) 6960–6969.
[17] A. Guskov, A. Gabdulkhakov, M. Broser, C. Glöckner, J. Hellmich, J. Kern, J. Frank, W. Saenger, A. Zouni, Recent progress in the crystallographic studies of Photosystem II, Chem. Phys. Chem. 11 (2010) 1160–1171.
[18] Y. Umena, K. Kawakami, J.-R. Shen, N. Kamiya, Crystal structure of oxygen-evolving photosystem II at a resolution of 1.9 Å, Nature 47 (2011) 55–60.
[19] R.I. Cukier, A theory that connects proton-coupled electron-transfer and hydrogen-atom transfer reactions, J. Phys. Chem. B 106 (2002) 1746–1757.
[20] S. Hammes-Schiffer, Hydrogen tunneling and protein motion in enzyme reactions, Acc. Chem. Res. 39 (2006) 93–100.
[21] M.H.V. Huynh, T.J. Meyer, Proton-coupled electron transfer, Chem. Rev. 107 (2007) 5004–5064.
[22] S.Y. Reece, D.G. Nocera, Proton-coupled electron transfer in biology: results from synergistic studies in natural and model systems, Annu. Rev. Biochem. 78 (2009) 673–699.
[23] R.A. Marcus, N. Sutin, Electron transfers in chemistry and biology, Biochim. Biophys. Acta 811 (1985) 265–322.
[24] C.C. Page, C.C. Moser, X. Chen, P.L. Dutton, Natural engineering principles of electron tunneling in biological oxidation-reduction, Nature 402 (1999) 47–52.
[25] G. Renger, G. Christen, M. Karge, H.-J. Eckert, K.-D. Irrgang, Application of the Marcus theory for analysis of the temperature dependence of the reactions leading to photosynthetic water oxidation — results and implications, J. Bioinorg. Chem. 3 (1998) 360–366.
[26] K. Kawakami, Y. Umena, N. Kamiya, J.-R. Shen, Structure of the catalytic, inorganic core of oxygen-evolving photosystem II at 1.9 Å resolution, J. Photochem. Photobiol. B: Biol 104 (2011) 9–18.
[27] G. Renger, H.-J. Eckert, W. Weiss, Studies on the mechanism of photosynthetic oxygen formation, in: Y. Inoue, A.R. Crofts, Govindjee, N. Murata, G. Renger, K. Satoh (Eds.), The Oxygen Evolving System in Photosynthesis, Academic Press, Japan, 1983, pp. 73–82.

[28] K. Brettel, E. Schlodder, H.T. Witt, Nanosecond reduction kinetics of photooxidized chlorophyll-a_{II} (P-680) in single flashes as a probe for the electron pathway, H^+-release and charge accumulation in the O_2-evolving complex, Biochim. Biophys. Acta 766 (1984) 403–415.

[29] H.-J. Eckert, G. Renger, Temperature dependence of $P680^+$ reduction in O_2-evolving PS II membrane fragments at different redox states S_i of the water oxidizing system, FEBS Lett. 236 (1988) 425–431.

[30] M.J. Schilstra, F. Rappaport, J.H.A. Nugent, C.J. Barnett, D.R. Klug, Proton/hydrogen transfer affects the S-state-dependent microsecond phases of $P680^+$ reduction during water splitting, Biochemistry 37 (1998) 3974–3981.

[31] M. Sugiura, F. Rappaport, K. Brettel, T. Noguchi, A.W. Rutherford, A. Boussac, Site-directed mutagenesis of *Thermosynechococcus elongatus* photosystem II: the O_2-evolving enzyme lacking the redox-active tyrosine D, Biochemistry 43 (2004) 13549–13563.

[32] P. Kühn, H.-J. Eckert, H.-J. Eichler, G. Renger, Analysis of the $P680^{+\cdot}$ reduction pattern and its temperature dependence in oxygen evolving PS II core complexes from thermophilic cyanobacteria and higher plants, Phys. Chem. Chem. Phys. 6 (2004) 4838–4843.

[33] R. Steffen, A.A. Kelly, H.-J. Eckert, P. Dörmann, G. Renger, Investigations on the reaction pattern of photosystem II in leaves from *Arabidopsis thaliana* wild type plants and mutants with genetically modified lipid content: II. Galactolipid deficiency, Biochemistry 44 (2005) 3123–3133.

[34] G. Renger, A.R. Holzwarth, Primary electron transfer, in: T. Wydrzynski, K. Satoh (Eds.), Photosystem II: The Water/ Plastoquinone Oxido-Reductase in Photosynthesis, Kluwer Academic Publishers, Dordrecht, The Netherlands, 2005, pp. 139–175.

[35] C. Jeans, M.J. Schilstra, D.R. Klug, The temperature dependence of $P680^+$ reduction in oxygen-evolving Photosystem II, Biochemistry 41 (2002) 5015–5023.

[36] G. Renger, H.-J. Eckert, M. Völker, Studies on the electron transfer from Tyr-161 of polypeptide D-1 to $P680^+$ in PS II membrane fragments from spinach, Photosynth. Res. 22 (1989) 247–256.

[37] M. Karge, K.-D. Irrgang, G. Renger, Analysis of the reaction coordinate of photosynthetic water oxidation by kinetic measurements of 355 nm absorption changes at different temperatures in photosystem II preparations suspended in either H_2O or D_2O, Biochemistry 36 (1997) 8904–8913.

[38] M. Karge, K.-D. Irrgang, S. Sellin, R. Feinäugle, B. Liu, H.-J. Eckert, H.-J. Eichler, G. Renger, Effects of hydrogen/deuterium exchange on photosynthetic water cleavage in PS II core complexes from spinach, FEBS Lett. 378 (1996) 140–144.

[39] A.M.A. Hayes, I.R. Vassiliev, J.H. Golbeck, R.J. Debus, Role of D1-His 190 in proton-coupled electron transfer reactions in photosystem II: a chemical complementation study, Biochemistry 37 (1998) 11352–11365.

[40] K. Saito, J.-R. Shen, T. Ishida, H. Ishikita, Short hydrogen bond between redox-active tyrosine Y_Z and D1-His190 in the Photosystem II crystal structure, Biochemistry 50 (2011) 9836–9844.

[41] Ö. Saygin, H.T. Witt, Evidence for the electrochromic identification of the change of charges in the four oxidation steps of the photoinduced water cleavage in photosynthesis, FEBS Lett. 187 (1985) 224–226.

[42] N. Ioannidis, G. Zahariou, V. Petrouleas, Trapping of the S_2 to S_3 state intermediate of the oxygen-evolving complex of Photosystem II, Biochemistry 45 (2006) 6252–6259.

[43] J.-H. Su, K.G.V. Havelius, F.M. Ho, G. Han, F. Mamedov, S. Styring, Formation spectra of the EPR split signals from the S_0, S_1, and S_3 states in Photosystem II induced by monochromatic light at 5 K, Biochemistry 46 (2007) 10703–10712.

[44] G. Renger, Photosynthetic water oxidation to molecular oxygen: apparatus and mechanism, Biochim. Biophys. Acta 1503 (2001) 210–228.

[45] J.S. Vrettos, J. Limburg, G.W. Brudvig, Mechanism of photosynthetic water oxidation: combining biophysical studies of photosystem II with inorganic model chemistry, Biochim. Biophys. Acta 1503 (2001) 229–245.

[46] H. Conjeaud, P. Mathis, The effect of pH on the reduction kinetics of *P*-680 in tris-treated chloroplasts, Biochim. Biophys. Acta 590 (1980) 353–359.

[47] G. Renger, M. Völker, W. Weiss, Studies on the nature of the water oxidizing enzyme. I. The effect of trypsin on the system II reaction pattern in inside-out thylakoids, Biochim. Biophys. Acta 766 (1984) 582–591.

[48] G. Christen, M. Karge, H.-J. Eckert, G. Renger, The role of protonation steps in electron transfer reactions in Tris-treated PS II membrane fragments, Photosynthetica 33 (1997) 529–539.

[49] R. Ahlbrink, M. Haumann, D. Cherepanov, O. Bögershausen, A. Mulkidjanian, W. Junge, Function of tyrosine Z in water oxidation by Photosystem II: electrostatical promotor instead of hydrogen abstractor, Biochemistry 37 (1998) 1131–1142.

[50] G. Renger, Role of hydrogen bonds in photosynthetic water splitting, in: K.-L. Han, G.J. Zhao (Eds.), Excited State Hydrogen Bonding and Hydrogen Transfer, Wiley Chichester, 2010, pp. 433–461.

[51] G. Renger, M. Völker, Studies on the proton release of the donor side of system II. Correlation between oxidation and deprotonization of donor D_1 in Tris-washed inside-out thylakoids, FEBS Lett. 149 (1982) 203–207.

[52] M. Sjödin, S. Styring, B. Åkermark, L. Sun, L. Hammarström, The mechanism for proton coupled electron transfer from tyrosine in a model complex and comparison with tyrosine Z oxidation in Photosystem II, Philos. Trans. B 357 (2002) 1471-1478.

[53] F. Rappaport, A. Boussac, D.A. Force, J. Peloquin, M. Brynda, M. Sugiura, S. Un, R.D. Britt, B.A. Diner, Probing the coupling between proton and electron transfer in Photosystem II core complexes containing a 3-fluorotyrosine, J. Am. Chem. Soc. 131 (2009) 4425–4433.

[54] G. Renger, W. Weiss, Functional and structural aspects of photosynthetic water oxidation, Biochem. Soc. Trans. 14 (1986) 17–20.

[55] P.J. van Leeuwen, C.C. Heimann, P. Gast, J.P. Dekker, H.J. van Gorkom, Flash-induced redox changes in oxygen-evolving spinach Photosystem II core particles, Photosynth. Res. 38 (1993) 169–176.

[56] F. Rappaport, M. Blanchard-Desce, J. Lavergne, Kinetics of the electron transfer and electrochromic change during the redox transitions of the photosynthetic oxygen-evolving complex, Biochim. Biophys. Acta 1184 (1994) 178–192.

[57] H. Koike, B. Hanssum, Y. Inoue, G. Renger, Temperature dependence of S-state transition in a thermophilic cyanobacterium, *Synechococcus vulcanus* Copeland, measured by absorption changes in UV region, Biochim. Biophys. Acta 893 (1987) 524–533.

[58] G. Renger, B. Hanssum, Studies on the reaction coordinates of the water oxidase in PS II membrane fragments from spinach, FEBS Lett. 299 (1992) 28–32.

[59] G. Renger, T. Bittner, J. Messinger, Structure–function relationship in photosynthetic water oxidation, Biochem. Soc. Trans. 22 (1994) 318–322.

[60] N. Lydakis-Simantiris, D.F. Ghanotakis, G.T. Babcock, Kinetic isotope effects on the reduction of the Y_Z radical in oxygen evolving and Tris washed photosystem II membranes by time resolved EPR, Biochim. Biophys. Acta 1322 (1997) 129–140.

[61] O. Bögershausen, M. Haumann, W. Junge, Photosynthetic oxygen evolution: H/D isotope effects and the coupling between electron and proton transfer during transitions S_2 to S_3 and S_3 to S_4 to S_0, Ber. Buns. Gesell. Chem, Phys. Phys. Chem. 100 (1996) 1987–1992.

[62] S. Styring, A.W. Rutherford, Deactivation kinetics and temperature dependence of the S-state transitions in the oxygen evolving system of photosystem II measured by EPR spectroscopy, Biochim. Biophys. Acta 933 (1988) 378–387.

[63] H. Koike, Y. Inoue, Temperature dependence of the S-state transitions in a thermophilic cyanobacterium measured by thermoluminescence, in: J. Biggins (Ed.), Progress in Photosynthesis Research, Nijhoff, Dordrecht, 1987, pp. 645–648.

[64] H.M. Gleiter, E. Haag, Y. Inoue, G. Renger, New results on the functional properties of a Photosystem II core complex preparation from spinach, Photosynth. Res. 35 (1993) 41–53.

[65] P. Joliot, A. Joliot, Different types of quenching involved in Photosystem II centers, Biochim. Biophys. Acta 305 (1973) 302–316.

[66] G. Renger, H.M. Gleiter, E. Haag, F. Reifarth, Photosystem II: thermodynamics and kinetics of electron transport from $Q_A^{-\bullet}$ to Q_B ($Q_B^{-\bullet}$) and deleterious effects of copper (II), Z. Naturforsch. 48c (1993) 234–240.

[67] F. Reifarth, G. Renger, Indirect evidence for structural changes coupled with $Q_B^{-\cdot}$ formation in Photosystem II, FEBS Lett. 428 (1998) 123–126.

[68] C. Fufezan, C. Zhang, A. Krieger-Liszkay, A.W. Rutherford, Secondary quinone in Photosystem II of *Thermosynechococcus elongatus*: semiquinone–iron EPR signals and temperature dependence of electron transfer, Biochemistry 44 (2005) 12780–12789.

[69] A. Garbers, J. Kurreck, F. Reifarth, G. Renger, F. Parak, Correlation between protein flexibility and electron transfer from $Q_A^{-\cdot}$ to Q_B in PS II membrane fragments from spinach, Biochemistry 37 (1998) 11399–11404.

[70] J. Pieper, G. Renger, Protein dynamics investigated by neutron scattering, Photosynth. Res. 102 (2009) 281–293.

[71] O. Kaminskaya, G. Renger, V.A. Shuvalov, Effect of dehydration on light induced reactions in Photosystem II: evidence for the presence of two functionally different Cytochromes b559, Biochemistry 42 (2003) 8119–8132.

[72] T. Noguchi, M. Sugiura, Flash-induced FTIR difference spectra of the water oxidizing complex in moderately hydrated Photosystem II core films: effect of hydration extent on S-state transitions, Biochemistry 41 (2002) 2322–2330.

[73] P. Chernev, I. Zaharieva, H. Dau, M. Haumann, Carboxylate shifts steer interquinone electron transfer in photosynthesis, J. Biol. Chem. 286 (2011) 5368–5374.

[74] H. Suzuki, M. Sugiura, T. Noguchi, Monitoring proton release during photosynthetic water oxidation in Photosystem II by means of isotope-edited infrared spectroscopy, J. Am. Chem. Soc. 131 (2009) 7849–7857.

[75] G. Renger, Light induced oxidative water splitting in photosynthesis: energetics, kinetics and mechanism, J. Photochem. Photobiol. B: Biol. 104 (2011) 35–43.

[76] D. Shevela, K. Beckmann, J. Clausen, W. Junge, J. Messinger, Membrane-inlet mass spectrometry reveals a high driving force for oxygen production by Photosystem II, Proc. Nat. Acad. Sci. 108 (2011) 3602–3607.

[77] G. Renger, Photosynthetic watersplitting : apparatus and mechanism, in: J. Eaton-Rye, Tripathy, T.D. Sharkey (Eds.), Photosynthesis: Photosynthesis:Plastid Biology, Energy Conversion and Carbon Assimilation, Springer, Dordrecht, The Netherlands, 2012, pp. 359–414.

[78] J. Messinger, G. Renger, Photosynthetic water splitting, in: G. Renger (Ed.), Primary Processes of Photosynthesis: Basic Principles and Apparatus, Reaction Centers/Photosystems, Electron Transport Chains, Photophosphorylation and Evolution., Vol. II, Royal Society Chemistry, Cambridge, 2008, p. 291-349.

[79] S. Schinzel, J. Schraut, A.-V. Arbuznikov, P.E.M. Siegbahn, M. Kaupp, Density functional calculations of ^{55}Mn, ^{14}N and ^{13}C electron paramagnetic rresonance parameters support an energetically feasible model system for the S2 state of the oxygen-evolving complex of Photosystem II, Chem. Eur. J. 16 (2010) 10424–10438.

[80] N. Cox, L. Rapatskiy, J.-H. Su, D.A. Pantazis, M. Sugiura, L. Kulik, P. Dorlet, A.W. Rutherford, F. Neese, A. Boussac, W. Lubitz, J. Messinger, Effect of Ca^{2+}/Sr^{2+} substitution on the electronic structure of the oxygen-evolving complex of Photosystem II: a combined multifrequency EPR, ^{55}Mn-ENDOR, and DFT study of the S_2 state, J. Am. Chem. Soc. 133 (2011) 3635-3648.

[81] P. Gatt, R. Stranger, R.J. Pace, Application of computational chemistry to understanding the structure and mechanism of the Mn catalytic site in photosystem II — a review, J. Photochem. Photobiol. B: Biol. 104 (2011) 80–93.

[82] P.E.M. Siegbahn, O – O bond formation in the S_4 state of the oxygen-evolving complex in photosystem, Chem. Eur. J. 12 (2006) 9217–9227.

[83] P.E.M. Siegbahn, Structures and energetics for O_2 formation in Photosystem II, Acc. Chem. Res. 42 (2009) 1871–1880.

[84] P.E.M. Siegbahn, Recent theoretical studies of water oxidation in photosystem II, J. Photochem. Photobiol B: Biol. 104 (2011) 94–99.
[85] V.L. Pecoraro, M.J. Baldwin, M.T. Caudle, W.-Y. Hsieh, N.A. Law, A proposal for water oxidation in photosystem II, Pure Appl. Chem. 70 (1998) 925–929.
[86] J. Messinger, Evaluation of different mechanistic proposals for water oxidation in photosynthesis on the basis of Mn_4O_xCa structures for the catalytic site and spectroscopic data, Phys. Chem. Chem. Phys. 6 (2004) 4764–4771.
[87] K. Meelich, C.M. Zaleski, V.L. Pecoraro, Using small molecule complexes to elucidate features of photosynthetic water oxidation, Philos. Trans. R. Soc. B 363 (2008) 1271–1281.
[88] J.P. McEvoy, G.W. Brudvig, Water-splitting chemistry of Photosystem II, Chem. Rev. 106 (2006) 4455–4483.
[89] Y. Pushkar, J. Yano, K. Sauer, A. Boussac, V.K. Yachandra, Structural changes in the Mn_4Ca cluster and the mechanism of photosynthetic water splitting, Proc. Natl. Acad. Sci. U. S. A. 105 (2008) 1879–1884.
[90] E.M. Sproviero, J.A. Gascon, J.P. McEvoy, G.W. Brudvig, V.S. Batista, Quantum mechanics/molecular mechanics study of the catalytic cycle of water splitting in Photosystem II, J. Am. Chem. Soc. 130 (2008) 3428–3442.
[91] G. Renger, Coupling of electron and proton transfer in oxidative water cleavage in photosynthesis, Biochim. Biophys. Acta 1655 (2004) 195–204.
[92] M. Haumann, P. Liebisch, C. Müller, M. Barra, M. Grabolle, H. Dau, Photosynthetic O_2 formation tracked by time-resolved X-ray experiments, Science (2005) 1019–1021.
[93] J. Clausen, R.J. Debus, W. Junge, Time-resolved oxygen production by PSII: chasing chemical intermediates, Biochim. Biophys. Acta 1655 (2004) 184–194.
[94] K. Strzalka, T. Walczak, T. Sarna, H.M. Swartz, Measurement of time-resolved oxygen concentration changes in photosynthetic systems by nitroxide-based EPR oximetry, Arch. Biochem. Biophys. 281 (1990) 312–318.
[95] M.R. Razeghifard, R.J. Pace, EPR kinetic studies of oxygen release in thylakoids in PSII membranes: a kinetic intermediate in the S_3 to S_0 transition, Biochemistry 38 (1999) 1252–1257.
[96] M. Hundelt, A.M.A. Hays, R.J. Debus, W. Junge, Oxygenic photosystem II: the mutationD1-D61N in *Synechocystis* sp. PCC 6803 retards S-state transitions without affecting electron transfer from Y_Z to $P680^+$, Biochemistry 37 (1998) 14450–14456.
[97] K.L. Westphal, N. Lydakis-Simantiris, R.I. Cukier, G.T. Babcock, Effects of Sr^{2+} substitution on the reduction rates of $Y_Z^{\bullet}$ in PSII membranes: evidence for concerted hydrogen atom transfer in oxygen evolution, Biochemistry 39 (2000) 16220–16229.
[98] E.H. Kim, R. Razeghifard, J.M. Anderson, W.S. Chow, Multiple sites of retardation of electron transfer in Photosystem II after hydrolysis of phosphatidylglycerol, Photosynth. Res. 93 (2007) 149–158.
[99] N. Ishida, M. Sugiura, F. Rappaport, T.-L. Lai, A.W. Rutherford, A. Boussac, Biosynthetic exchange of bromide for chloride and strontium for calcium in the Photosystem II oxygen-evolving enzymes, J. Biol. Chem. 283 (2008) 13330–13340.
[100] G. Renger, Oxidative photosynthetic water splitting: energetics, kinetics and mechanism, Photosynth. Res. 92 (2007) 407–425.
[101] M. Kusunoki, S_1-state Mn_4Ca complex of Photosystem II exists in equilibrium between the two most-stable isomeric substates: XRD and EXAFS evidence, J. Photochem. Photobiol. B: Biol. 104 (2011) 100–110.
[102] T. Ono, H. Nakayama, H. Gleiter, Y. Inoue, A. Kawamori, Modification of the properties of S_2 state in photosynthetic O_2-evolving center by replacement of chloride with other anions, Arch. Biochem. Biophys. 256 (1987) 618–624.
[103] A. Haddy, W.R. Dunham, R.H. Sands, R. Aasa, Multifrequency EPR investigations into the origin of the S_2-state signal at $g=4$ of the O_2-evolving complex, Biochim. Biophys. Acta 1099 (1992) 25–34.
[104] P. van Vliet, A.W. Rutherford, Properties of the chloride-depleted oxygenevolving complex of photosystem II studied by electron paramagnetic resonance, Biochemistry 35 (1996) 1829–1839.
[105] A. Boussac, A.W. Rutherford, Comparative study of the $g=4.1$ EPR signals in the S_2 state of photosystem II, Biochim. Biophys. Acta 1457 (2000) 145–156.
[106] M. Chrysina, G. Zahariou, Y. Sanakis, N. Ioannidis, V. Petrouleas, Conformational changes of the $S_2Y_Z^{\bullet}$ intermediate of the S_2 to S_3 transition in photosystem II, J. Photochem. Photobiol. B: Biol. 104 (2011) 72–79.
[107] G. Chen, G. Han, E. Göransson, F. Mamedov, S. Styring, Stability of the S_3 and S_2 state intermediates in Photosystem II directly probed by EPR spectroscopy, Biochemistry 51 (2012) 138–148.
[108] R. Debus, The catalytic manganese cluster: protein ligation, in: T. Wydrzynski, K. Satoh (Eds.), Photosystem II: The Water/ Plastoquinone Oxido-Reductase in Photosynthesis, Kluwer Academic Publishers, Dordrecht, The Netherlands, 2005, pp. 261–284.
[109] Y. Shimada, H. Suzuki, T. Tsuchiya, T. Tomo, T. Noguchi, M. Mimuro, Effect of a single-amino acid substitution of the 43 kDa chlorophyll protein on the oxygen-evolving reaction of the cyanobacterium *Synechocystis* sp. PCC 6803: Analysis of the Glu354Gln mutation, Biochemistry 48 (2009) 6095–6103.
[110] R.J. Service, J. Yano, I. McConnell, H.J. Hwang, D. Niks, R. Hille, T. Wydrzynski, R.L. Burnap, W. Hillier, R.J. Debus, Participation of glutamate-354 of the CP43 polypeptide in the ligation of manganese and the binding of substrate water in Photosystem II, Biochemistry 50 (2011) 63–81.
[111] N. Ishida, M. Sugiura, F. Rappaport, T.-L. Lai, A.W. Rutherford, A. Boussac Biosynthetic, exchange of bromide for chloride and strontium for calcium in the Photosystem II oxygen-evolving enzymes, J. Biol. Chem. 283 (2008) 13330–13340.
[112] F. Rappaport, N. Ishida, M. Sugiura, A. Boussac, Ca^{2+} determines the entropy changes associated with the formation of transition states during water oxidation by Photosystem II, Energy Environ. Sci. 4 (2011) 2520–2524.
[113] G. Renger, The action of 2-anilinothiophenes as accelerators of the deactivation reactions in the water splitting enzyme system of photosynthesis, Biochim. Biophys. Acta 256 (1972) 428–439.
[114] G. Renger, G. Bouges-Bocquet, R. Delosme, Studies on the ADRY-agent induced mechanism of the discharge of the holes trapped in the photosynthetic water splitting enzyme system, Biochim. Biophys. Acta 292 (1973) 796–807.
[115] G. Renger, Y. Inoue, Studies on the mechanism of ADRY-agents on the thermoluminescence emission, Biochim. Biophys. Acta 725 (1983) 146–154.
[116] B. Hanssum, G. Dohnt, G. Renger, On the mechanism of ADRY agent — interaction with the PS II donor side, Biochim. Biophys. Acta 806 (1985) 210–220.
[117] T. Ono, J.L. Zimmermann, Y. Inoue, A.W. Rutherford, EPR evidence for a modified S-state transition in chloride-depleted Photosystem II, Biochim. Biophys. Acta 851 (1986) 193–201.
[118] P.H. Homann, H. Gleiter, T. Ono, Y. Inoue, Storage of abnormal oxidants '$\sum_1$', '$\sum_2$' and '$\sum_3$' in photosynthetic water oxidases inhibited by Cl^--removal, Biochim. Biophys. Acta 805 (1986) 10–20.
[119] H. Wincencjusz, H.J. van Gorkom, C.F. Yocum, The photosynthetic oxygen evolving complex requires chloride for its redox state $S_2 \rightarrow S_3$ and $S_3 \rightarrow S_0$ transitions but not for $S_0 \rightarrow S_1$ or $S_1 \rightarrow S_2$ transitions, Biochemisty 36 (1997) 3663–3670.
[120] H. Wincencjusz, H.J. van Gorkom, C.F. Yocum, Activating anions that replace Cl^- in the O_2-eevolving complex of Photosystem II slow the kinetics of the terminal step in water oxidation and destabilize the S_2 and S_3 States, Biochemisty 38 (1999) 3719–3725.
[121] T. Noguchi, FTIR detection of water reactions in the oxygen-evolving centre of photosystem II, Philos. Trans. R. Soc. B 363 (2008) 1189–1195.
[122] Y. Shimada, H. Suzuki, T. Tsuchiya, M. Mimuro, T. Noguchi, Structural coupling of an arginine side chain with the oxygen-evolving Mn_4Ca cluster in Photosystem II as revealed by isotope-edited Fourier Transform Infrared Spectroscopy, J. Am. Chem. Soc. 133 (2011) 3808–3811.
[123] G. Renger, P. Kühn, Reaction pattern and mechanism of light induced oxidative water splitting in photosynthesis, Biochim. Biophys. Acta 1767 (2007) 458–471.
[124] M.M. Najafpour, Mixed-valence manganese calcium oxides as efficient catalysts for water oxidation, Dalton Trans. 40 (2011) 3793–3795.
[125] G. Renger, Mechanistic aspects of photosynthetic water cleavage, Photosynthetica 21 (1987) 203–224.
[126] T. Saito, S. Yamanaka, K. Kanda, H. Isobe, Y. Takano, Y. Shigeta, Y. Umena, K. Kawakami, J.-R. Shen, N. Kamiya, M. Okumura, M. Shoji, Y. Yoshioka, K. Yamaguchi, Possible mechanisms of water splitting reaction based on proton and electron release pathways revealed for $CaMn_4O_5$ cluster of PSII refined to 1.9 Å X-ray resolution, Int. J. Quant. Chem. 112 (2012) 253–276.